

Design, Implementation and Control of  
Rehabilitation Robots  
for Upper and Lower Limbs

by

Mehmet Alper Ergin

Submitted to the Graduate School of Sabancı University  
in partial fulfillment of the requirements for the degree of  
Master of Science

Sabancı University

August, 2011

Design, Implementation and Control of Rehabilitation Robots  
for Upper and Lower Limbs

APPROVED BY:

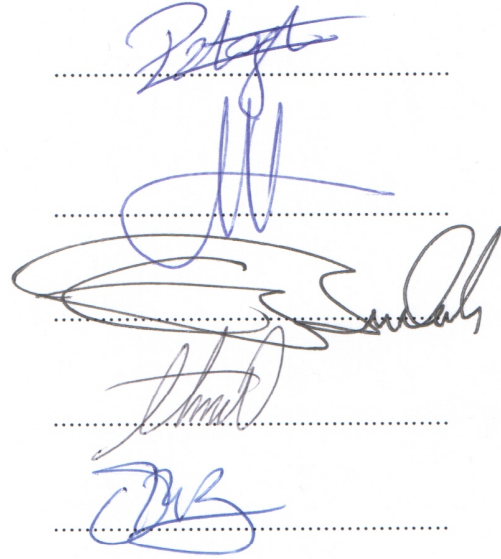
Assist. Prof. Dr. Volkan Patođlu  
(Thesis Advisor)

Assoc. Prof. Dr. Mahmut Akřit

Prof. Dr. Erhan Budak

Assist. Prof. Dr. Ahmet Onat

Assist. Prof. Dr. Gll Kızıldař řendur

Handwritten signatures in blue ink, corresponding to the names listed on the left. The signatures are written over horizontal dotted lines.

DATE OF APPROVAL:

09.08.2011

© Mehmet Alper Ergin, 2011

All Rights Reserved

# Design, Implementation and Control of Rehabilitation Robots for Upper and Lower Limbs

Mehmet Alper Ergin

ME, Master of Science, 2011

Thesis Supervisor: Assist. Prof. Dr. Volkan Patođlu

Keywords: Robotic Rehabilitation, Series Elastic Actuation, Force Feedback Exoskeleton, Holonomic Platform, Passive Velocity Field Control.

## Abstract

We present two novel rehabilitation robots for stroke patients. For lower limb stroke rehabilitation, we present a novel self-aligning exoskeleton for the knee joint. The primal novelty of the design originates from its kinematic structure that allows translational movements of the knee joint on the sagittal plane along with the knee rotation. Automatically adjusting its joint axes, the exoskeleton enables a perfect match between human joint axes and the device axes. Thanks to this feature, the knee exoskeleton is not only capable of guaranteeing ergonomy and comfort throughout the therapy, but also extends the usable range of motion for the knee joint. Moreover, this adjustability feature significantly shortens the setup time required to attach the patient to the robot, allowing more effective time be spend on exercises instead of wasting it for adjustments. We have implemented an impedance-type concept of the knee exoskeleton, experimentally characterized its closed-loop performance and demonstrated ergonomy and useability of this device through human subject experiments.

To administer table top exercises during upper limb stroke rehabilitation, we present a novel Mecanum-wheeled holonomic mobile rehabilitation robot for home therapy. The device can move/rotate independently on its unlimited planar workspace to provide assistance to patients. We have implemented two different concepts of holonomic mobile platform based on different actuation and sensing principles: an admittance-type mobile robot and a mobile platform with series elastic actuation. The admittance-type robot is integrated with virtual reality simulations and can assist patients through virtual tunnels designed around nominal task trajectories. The holonomic platform with series elastic actuation eliminates the need for costly force sensors and enables implementation of closed loop force control with higher controller gains, providing robustness against imperfections in the power transmission and allowing lower cost drive components to be utilized. For contour following tasks with the holonomic platforms, we have synthesized passive velocity field controllers (PVFC) that ensure coordination and synchronization between various degrees of freedom of the patient arm, while letting patients to complete the task at their own preferred pace. PVFC not only minimizes the contour error but also ensures coupled stability of the human-in-the-loop system.

# Üst ve Alt Ekstrimite Rehabilitasyon Robotlarının Tasarımı, Uygulaması ve Kontrolü

Mehmet Alper Ergin

Yüksek Lisans Tezi, 2011

Tez Danışmanı: Yrd. Doç. Dr. Volkan Patoğlu

Anahtar kelimeler: Robot Destekli Rehabilitasyon, Seri-Elastik Eyleyici, Kuvvet Geri-Beslemeli Dış-İskelet, Holonomik Platform, Pasif Hız Alanı Kontrolü.

## Özetçe

Bu tezde inme hastaları için iki yeni rehabilitasyon robotu sunuyoruz. Alt-ekstrimite inme rehabilitasyonunda diz eklemi için kendiliğinden hizalanabilen bir dış-iskelet sunmaktayız. Tasarımın ana yeniliği sağıtal düzlemde dönme hareketleriyle beraber öteleme hareketlerini de gerçekleştirebilmeye olanak tanıyan kinematik yapısından kaynaklanmaktadır. Kendiliğinden hizalanabilme özelliğı insan ve robot eklemleri arasında kusursuz bir uyum sağlamaktadır. Bu özellik sayesinde diz dış-iskeleti, terapi süresince ergonomi ve konfor sağlamanın yanı sıra diz ekleminin kullanılabilir hareket alanını da arttırmaktadır. Ayrıca, kendiliğinden hizalanabilme özelliğı terapi öncesi hastayı robota bağlamak için harcanan kurulum süresini kısaltmakta ve terapi süresinden daha fazla verim alınmasına olanak tanımaktadır.

Sunulan diz dış-iskeletini empedans-tipi kavramı ile birleştirdik ve kapalı-döngü performansını deneysel olarak karakterize ettik. Robotun ergonomisini ve işlevselliğini insan deneyleri üzerinden gösterdik.

Üst-ekstrimite inme rehabilitasyonu için masa üzeri hareketlerini ev ortamında yapabilmeyi sağlayan Mecanum tekerlekli holonomik, gezgin bir platform sunmaktayız. Cihaz limitsiz çalışma alanında dönme ve ilerleme hareketlerini bağımsız olarak yapabilmekte ve hastaya destekleyici kuvvetler uygulayabilmektedir. Robotun, admitans tipi ve seri-elastik eyleyiciye sahip olmak üzere, farklı çalıştırılma tekniklerine dayanan iki ayrı tasarım kavramını ürettik. Admitans tipi robotu hastaya destek verebilen, sanal tünellere dayalı sanal gerçeklik uygulamaları ile birleştirdik. Seri-elastik eyleyiciye sahip holonomik platform tasarımı ile yüksek maliyetli kuvvet sensörlerine olan ihtiyacı ortadan kaldırıp robot üzerinde yüksek kazanıma sahip kapalı döngü kuvvet kontrolü uygulanabilmesini mümkün kıldık. Bu sayede güç aktarım elemanlarında olabilecek mekanik hatalara karşı gürbüzlük sağlayıp düşük maliyetli parça kullanımına imkan verdik.

Holonomik platforma rota takip etme uygulamaları için koordinasyon ve senkronizasyonu sağlarken hastanın uygulamayı kendi temposu içerisinde tamamlamasına olanak tanıyan pasif hız alanı kontrolörü (PVFC) sentezledik. PVFC rota hatalarını küçültmenin yanı sıra döngü içerisinde insan olan sistemlerin kararlı olmasını da garantilemektedir.

## Acknowledgements

It is a great pleasure to extend my gratitude to my thesis advisor Assist. Prof. Dr. Volkan Patođlu for his precious guidance and support. I am greatly indebted to him for his supervision and excellent advises throughout my Master study. I would gratefully thank Assoc. Prof. Dr. Mahmut Faruk Akřit, Prof. Dr. Erhan Budak, Assist. Prof. Dr. Ahmet Onat and Assist. Prof. Dr. Gll Kızıltaş řendur for their feedbacks and spending their valuable time to serve as my jurors.

I would like to acknowledge the support provided by Marie Curie Rehab Duet research grant and Sabanci University for waiving the tuition throughout my master study.

I am heartily thankful to Ahmetcan Erdođan and Ozan Tokatlı for their support and invaluable help. Many thanks to my friends, Aykut Cihan Satıcı, Melda Ulusoy, Can Palaz, Kadir Haspalamutgil, Hakan Ertaş, Elif Hocoaođlu, Neře Tfekçiler, Ali Utku Pehlivan and Mustafa Yalçın for making the laboratory enjoyable and memorable. Thanks to Mehmet Gler and Sleyman Tutkun for their precious support throughout my research and for sharing their experience and technical knowledge.

I owe my deepest gratitude to my family for all their love and support throughout my life. Finally, I would like to express my love and gratitude to Elif Yılmaz, without her love, support and empathise this research would not have been possible.

# Contents

<b>1</b>	<b>Introduction</b>	<b>1</b>
1.1	Motivation . . . . .	1
1.1.1	Stroke Rehabilitation . . . . .	1
1.2	Robot Assistance for Stroke Therapy . . . . .	3
1.2.1	Lower Limb Rehabilitation Robots . . . . .	4
1.2.2	Upper Limb Rehabilitation Robots . . . . .	8
1.3	Contributions . . . . .	13
1.4	Outline of the Thesis . . . . .	16
<b>2</b>	<b>Design of Rehabilitation Robots</b>	<b>17</b>
2.1	Design Criteria . . . . .	17
2.1.1	Lower Limb Rehabilitation Robot . . . . .	18
2.1.2	Upper Limb Rehabilitation Robot . . . . .	19
2.2	Kinematic Type Selection . . . . .	20
2.2.1	Lower Limb Rehabilitation Robot . . . . .	20
2.2.2	Upper Limb Rehabilitation Robot . . . . .	21
2.3	Conceptual Designs . . . . .	23
2.3.1	Knee Exoskeleton . . . . .	24
2.3.2	Holonomic Mobile Platform . . . . .	31
2.4	Kinematics . . . . .	35
2.4.1	Kinematics of the Knee Exoskeleton . . . . .	35
2.4.2	Kinematics of the Holonomic Mobile Platform . . . . .	41
2.5	Dynamics . . . . .	45
2.5.1	Dynamics of the Knee Exoskeleton . . . . .	45
2.5.2	Dynamics of the Mobile Platform . . . . .	46

<b>3</b>	<b>Implementation</b>	<b>47</b>
3.1	Implementation of the Knee Exoskeleton . . . . .	47
3.2	Implementation of the Holonomic Platform . . . . .	49
3.2.1	Concept I: Holonomic Platform with F/T Sensor . . . . .	49
3.2.2	Concept II: Holonomic Platform with SEA . . . . .	52
<b>4</b>	<b>Controller Synthesis, Characterization and VR Integration</b>	<b>64</b>
4.1	Control of the Knee Exoskeleton . . . . .	64
4.1.1	Impedance Controller . . . . .	64
4.1.2	Human Subject Experiments . . . . .	68
4.2	Control of the Mobile Platform . . . . .	71
4.2.1	Admittance Control . . . . .	71
4.2.2	Series Elastic Actuation . . . . .	73
4.2.3	Passive Velocity Field Controller . . . . .	74
4.2.4	Virtual Reality Integration of the Mobile Platform . . . . .	80
4.3	Experimental Characterization . . . . .	81
4.3.1	Experimental Characterization of the Knee Exoskeleton . . . . .	81
4.3.2	Experimental Characterization of the Mobile Platform . . . . .	82
<b>5</b>	<b>Conclusions and Future Work</b>	<b>85</b>
5.1	The Knee Exoskeleton . . . . .	85
5.2	Holonomic Mobile Platform . . . . .	86

## List of Figures

1.1	Lower limb rehabilitation robots . . . . .	5
1.2	Anterior-posterior translation . . . . .	7
1.3	Fixed base upper limb rehabilitation robots . . . . .	10
1.4	Mobile upper limb rehabilitation robots . . . . .	11
2.1	Selected Type for Upper Limb Robot . . . . .	22
2.2	Selected Type for Upper Limb Robot . . . . .	23
2.3	Impedance Controlled Design . . . . .	25
2.4	Knee robot with built in F/T sensing . . . . .	26
2.5	Force sensor dynamics effects . . . . .	27
2.6	SEA design of the knee robot . . . . .	29
2.7	VSA design of the knee exoskeleton . . . . .	30
2.8	Mobile Platform with built in F/T sensing . . . . .	32
2.9	Mobile Platform with SEA force sensing . . . . .	34
2.10	CAD of 3- <u>RRP</u> mechanism . . . . .	35
2.11	CAD Model of Mobile Platform . . . . .	42
3.1	Prototype of 3- <u>RRP</u> mechanism . . . . .	48
3.2	Exoskeleton prototype attached to knee . . . . .	50
3.3	Holonomic Platform with F/T Sensor . . . . .	51
3.4	Top view of the HMP with SEA . . . . .	53
3.5	Front view of the HMP with SEA . . . . .	54
3.6	CAD model of notch-hinge compliant joint . . . . .	56
3.7	Top view of the compliant SEA . . . . .	59
3.8	Human connection to the HMP with SEA . . . . .	60
3.9	Experimental verification of SEA on x . . . . .	62
3.10	Experimental verification of SEA on y . . . . .	62

3.11	Experimental verification of SEA on rotations. . . . .	63
4.1	Block diagram of the impedance control architecture . . . . .	65
4.2	Knee exoskeleton path tracking performance . . . . .	66
4.3	Force rendering performance of knee exoskeleton . . . . .	67
4.4	Human subject I . . . . .	69
4.5	Human subject II . . . . .	69
4.6	Human subject III . . . . .	70
4.7	Block diagram of the admittance controller . . . . .	72
4.8	Block diagram of SEA control . . . . .	73
4.9	PVFC simulation results in x-direction . . . . .	78
4.10	PVFC simulation results in y-direction . . . . .	79
4.11	PVFC simulation results in task space . . . . .	79
4.12	Table Game . . . . .	80
4.13	Virtual Tunnel . . . . .	84

## List of Tables

4.1	Characterization Table for the 3- <u>RRP</u> Knee Exoskeleton . . .	81
4.2	Characterization Table for the HMP with F/T Sensor . . . . .	82
4.3	Characterization Table for the HMP with SEA . . . . .	83

# Chapter I

## 1 Introduction

We start by motivating robot assisted rehabilitation for treatment of stroke patients. Then, robotic devices developed for upper and lower limb stroke rehabilitation are discussed. The introduction continues by detailing the contributions of the thesis and concludes with the outline.

### 1.1 Motivation

In this section, stroke rehabilitation and its burden on both therapists and economy are discussed and main notions of upper and lower limb rehabilitation are presented.

#### 1.1.1 Stroke Rehabilitation

Neurological injuries are the leading cause of serious, long-term disability [1]. Each year about 15 million people suffer a stroke. According to the National Stroke Association of US, the estimated the cost per patient, in the first 3 months of treatment is about 15 thousands U.S dollars, although for 10% of cases cost are higher than 35 thousand U.S dollars [2]. The situation gets even more serious with the ageing of the population, in particular, in the EU countries and Japan. Physical rehabilitation therapy is indispensable for treating neurological disabilities.

The notion of physical therapies differs with the body part that is in consideration. As an example, targeted joint exercises are more emphasized during the lower limb therapies, since natural gait movements can only be realized with proper motion of the joints. All the joints of the lower limb have complex structures. In particular, hip, knee and ankle all possess more than one degree of freedom (DoF). In order to sustain a natural gait, the therapeutic exercises for these joints should allow for the movements along each natural DoF. On the other hand, during therapy sessions for the upper limb rehabilitation, reaching exercises, such as pick and place tasks, are more commonly administered. During these exercises, resulting movements in the task space become more emphasized, compared to the isolated movement of each joint.

### **Lower Limb Rehabilitation**

It is well recognized in the biomechanics literature that many of the human joints have complex movements, such that rotations of the joints are strongly coupled with the translation of the rotation axes. Unfortunately, many of the existing rehabilitation robots neglect this coupling and model human joints as a collection of simple hinges with pure rotary movements. One of the recent trends in the design of rehabilitation robots, especially for exoskeleton-types, is to accommodate complex movements of the joints [3, 4]. Although the robot assisted rehabilitation for lower limbs has been well studied, the complex movements of the joints have not been considered in detail. In this thesis, the joint alignment problem for the knee joint is identified and a solution for the proper alignment of the knee joint with the robot axes is presented.

## Upper Limb Rehabilitation

The exercises used during the upper limb rehabilitation with robot assistance usually aims to increase the effective range of motion of the patient arm. An effective way of increasing the range of motion is to administer reaching motions to the patient. The human arm is capable of realizing motions in a six dimensional space: three DoF translations and three DoF rotations. However, many practical task in our daily lives require reaching movements on a plane. As a result, table top exercises, during which the weight of the arm is supported by the planar constraint, are widely administered as upper limb rehabilitation exercises. In this thesis, an active robotic device is designed and implemented for providing assistance to stroke patients while performing table top reaching exercises.

### 1.2 Robot Assistance for Stroke Therapy

Physical therapy is an indispensable element in treating disabilities secondary to neurological disorders. Treatment is more effective when exercises are repetitive [5], intense [6], long term [7] and task specific [8]. On the other hand, such therapies are costly due to large amount of manual labor necessary to implement them. Use of robotic devices in assistance of repetitive and physically involved rehabilitation exercises decrease the physical burden of therapists, while also significantly reducing the application related costs. Moreover, robot-mediated rehabilitation therapy allows quantitative measurements of patient progress, guarantees patient safety, and increase accuracy of tasks with high repetitions, and can be utilized to realize customized, interactive treatment protocols. Effectiveness of robotic rehabili-

tation for treatment of neurological injuries has been demonstrated through many clinical trials [9–12].

Over the last decade, research on rehabilitation robots has primarily focused on enabling active involvement of the patients by designing back-driveable robots [13, 14] and deriving control algorithms that assist patients only as much as needed [15, 16]. To this end, the transition from highly rigid continuous passive motion devices [17, 18] to back-driveable robots with adjustable impedances [19, 20] and from position control algorithms in which the patient is viewed as a disturbance to shared control approaches that promote active involvement of patients [21, 22] have significantly increased efficacy of robot assisted therapies.

The rehabilitation robots used in clinical therapy can be loosely categorized into two: lower limb rehabilitation robots and upper rehabilitation limb robots. The primary aim of lower limb rehabilitation robots is to help patients regain their locomotion capabilities, while upper limb rehabilitation robots focus helping patients regain stable reaching movements.

### **1.2.1 Lower Limb Rehabilitation Robots**

The design of robotic systems for lower limb rehabilitation is an attractive research area since the human biomechanics during gait cycle possess complex motions. There have been successful implementations of full leg exoskeletons for lower limb rehabilitation and even commercial devices exist as in Figure 1.2.1. Most well-known of these devices, Lokomat [23, 24], employs a DC motor driven simple revolute joint at its knee joint. Another well known gait rehabilitation robot, LOPES gait trainer [25], utilizes series elasticity to measure forces acting on the knee joint but still models the kinematics of

human knee as a pure rotary motion. The ERF knee [26], a joint specific, portable mechanisms for knee exercises, is based on an electro-rheological fluid rotary actuator which also employs a simple hinge model for the knee. In order to implement natural feeling gait movements, the joint axes of exoskeletons should perfectly correspond with the human joint. The lower limb exoskeletons mentioned above have proper mechanisms that enable such a correspondence with the hip joint. However, all these robots model knee joint as simple hinge joint, neglecting the complex movement of the knee goes through during a gait cycle. The problems of modeling the knee joint



Figure 1.1: Lower limb rehabilitation robots: Lokomat, Lopes and ERF knee respectively

as a simple revolute joint have been revised much earlier in the design of prosthetic and orthotics devices. Unlike the case with the active rehabilitation robots, the complex movement of the knee is widely acknowledged in this field and such movements have already been integrated in the design of most prosthetics and orthotics devices. For instance, the Jaipur knee [27], a knee prosthesis designed for amputees, mimics the movements of human knee by changing its center of rotation during movement. Similarly, in [28] self-adjusting orthoses has been proposed for rehabilitation of knee joint. Note that prosthetics and orthotics devices are passive; hence, cannot be used to assist patients to complete rehabilitation exercises.

Even though movement of complex joints have been intensely studied in

the biomechanics literature, design of rehabilitation robots that enable such movements is a recent challenge. In the rehabilitation robotic literature, complex movements of the knee joint have not been addressed; however, there exist recent studies that focus on rehabilitation of other complex joints, such as the shoulder joint. These studies are briefly reviewed in the next section.

### **Robotic Rehabilitation of Complex Joints**

An exoskeleton-type rehabilitation robot should fully correspond with the movements of human joint to sustain uncompensated, natural feeling, ergonomic movements. In the literature, the importance of the joint correspondence, to sustain ergonomics, has been first noticed for the design of the shoulder joint as the center of rotation of the shoulder joint changes significantly during arm movements. The need for extra degrees of freedom (DoF) has been first proposed in [29]. Later, a fully articulated passive shoulder mechanism has been introduced in [3]. Translational movements of the shoulder joint has been addressed for actuated full arm exoskeletons in [30]. The upper-arm exoskeleton ARMin I [31] has been reported to be uncomfortable with limited useable range, since this exoskeleton is based on simplified model of the five DoF shoulder; a model that views shoulder as a simple spherical joint. As a result, in [32, 33] enhanced versions of ARMin have been proposed to provide better approximations to the coupled movement of the shoulder joint. Coupled motion of the shoulder joint is also addressed in [34] by utilizing high DoF devices and in [4] by using self-aligning mechanisms.

As in the case with the shoulder joint, the knee is a complex joint with theoretically up to 6 DoF. On the other hand, biomedical studies indicate that important components of the movement take place in the sagittal plane

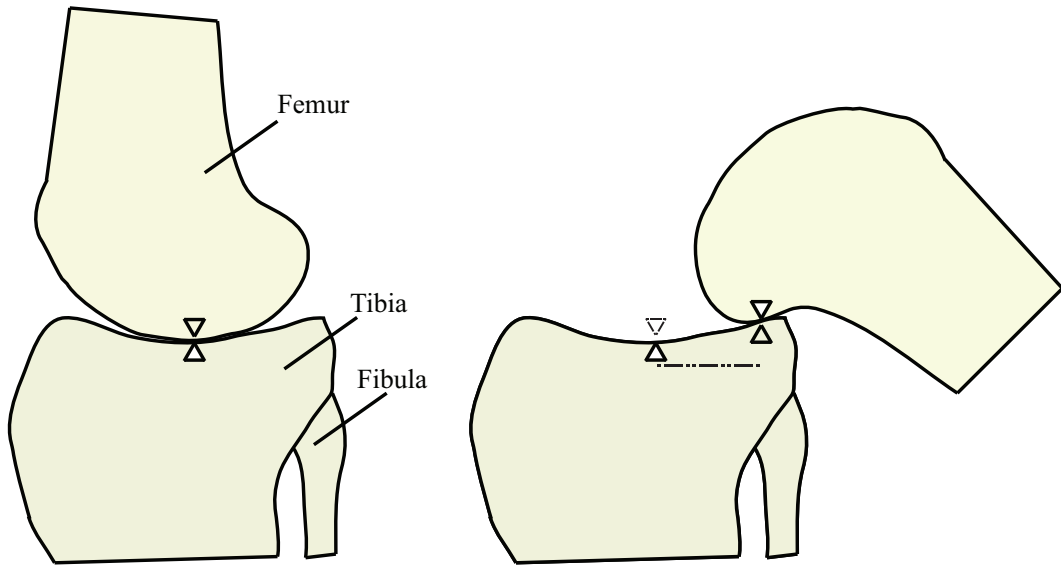


Figure 1.2: A schematic representation of sagittal plane anterior-posterior translation during flexion/extension movement of the knee joint

while out of plane the movements of the knee are mostly constrained with bony and ligamentous structures [35] and can be neglected. On the sagittal plane, the rotation axis of the knee joint translates significantly during knee flexion and extension. The translation of the joint axis, called anterior-posterior translations, is depicted in Figure 1.2. The kinematic models of the knee as well as experimental data suggest that the magnitude of anterior-posterior translations can exceed 19 mm for a healthy human [36]. The amount of translation changes with flexion and extension angle and is unique to every individual, since it strongly depends on the size and orientation of the bones and the shape of articulated surfaces. Moreover, in practice, the alignment of human joint with robot axis cannot be handled precisely, since the exact joint center of human cannot be determined from outside the body [4].

## **Proposed Knee Exoskeleton**

In the thesis, a self-adjusting knee exoskeleton for robot-assisted treatment of knee injuries is presented. The primal novelty of the proposed device originates from its kinematic structure that allows translational movements of the knee joint on the sagittal plane along with the knee rotation. The elastic attachment part of the robot enables passive knee internal/external rotations, enabling a perfect match between human joint axes and the device axes. Automatically adjusting its joint axes, the proposed device is not only capable of guaranteeing ergonomy and comfort throughout the therapy, but also extends the usable (comfortable) range of motion for the knee joint. Moreover, adjustability feature significantly shortens the setup time required to attach the patient to the robot, allowing more effective time be spend on exercises instead of wasting it for adjustments. The proposed system is different from the similar works in literature in that it supports both passive translational movements of the knee joint and independent active control of these degrees of freedom. Sustaining active and passive alignment of the knee joint increases the number of applicable therapy protocols. In particular, the therapist can impose sessions involving the control knee flexion/extension movements by letting the knee to adjust the remaining DoF passively. In the case of ligamentous structure injuries, the robot can apply active alignment of the inherently passive movements of the knee to enforce and support the natural movement trajectories of the joint.

### **1.2.2 Upper Limb Rehabilitation Robots**

Robots designed for upper limb rehabilitation can be loosely categorized into two as exoskeleton and end-effector type devices. Exoskeleton type robots

correspond with human joints; therefore, are effective in delivering specific joint therapies. In particular, exoskeletons are capable of applying controlled torques to individual joints and measuring the movements of specific joints decoupled from movements of other joints. Many successful implementations of exoskeleton type upper limb rehabilitation robots have been developed in the literature, including [33,37–40]. In spite of the advantages of exoskeleton type robots, utilization of these devices are not always feasible, since due to inherent mechanical complexity in their designs, exoskeleton robots are very expensive. The end-effector type upper limb rehabilitation robots can be further categorized into two as fixed based and mobile upper limb rehabilitation robots.

### **Fixed Based Upper Limb Rehabilitation Robots**

End-effector type rehabilitation robots do not correspond with human joints, but administer controlled therapeutic movements at the end-effector of the device, where the human is attached. Therefore, without external restraints on the joints, joint specific therapies are not achievable by such mechanisms. However, end-effector type robots are advantageous thanks to their simple kinematic structure and low cost. Moreover, many of these devices are portable and suitable for home based therapy. With respect to their portability characteristics, end-effector type rehabilitation robots can further be categorized into fixed-base and mobile devices. A well-known example of fixed-base robots is the MIT-Manus [41], seen in Figure 1.2.2. MIT-Manus is an impedance-type robot that possesses two grounded direct-drive motors to provide torques to assist or resist patient movements. Another example of fixed-base devices is Gentle/s [42], which uses an admittance-type robot



Figure 1.3: Fixed based upper limb rehabilitation robots: MIT-Manus and Gentle/s respectively

(HapticMaster) [43] along with a gimbal mechanism to connect to the human wrist. Reha-Slide is another fixed base device which is designed to administer resistive movement therapies [44]. Even though fixed-based end-effector type rehabilitation robots have been shown to be effective in delivering therapies in a clinical setting, their adaptation for home-based therapy is not very feasible.

### Mobile Upper Limb Rehabilitation Robots

In contrast to the fixed-base devices, rehabilitation robots based on mobile platforms can be designed to be light and compact; therefore, such devices hold high promise for enabling home based robotic therapy. Since these devices can be implemented with much lower manufacturing costs, their widespread availability becomes feasible. Several low-cost, home-based rehabilitation robots have been designed in the literature. A well-known low-cost, mobile device is the arm skate [45], seen in Figure 1.2.2, which is a passive device equipped with reed-relays and magnets. In this robot, reed relays are utilized to link objects defined in a virtual environment with the physical environment and to determine the robot position. A later implementation of



Figure 1.4: Mobile upper limb rehabilitation robots: Arm-skate, Rutgers arm and system with Wii remote respectively

this robot excludes reed-relays in favor of electromagnetic brakes to provide resistance to the patients whenever required [46]. Another example of low-cost table-top devices is the Rutgers Arm II [47], a mobile device that uses teflon balls to slide over a table. In order to provide assistance or resistance to the patient, the table is manually tilted to employ gravity to provide the required power. Unfortunately, manual use of gravity field restricts the available assistance/resistance that can be provided to a very limited spectrum. Other low-cost systems include use of Wii remote and infrared cameras along with virtual reality games, such as pick-and-place tasks [48].

### Proposed Mobile Platform

In this thesis, we propose utilizing a holonomic mobile platform to administer therapeutic table-top exercises to patients who have suffered injuries that affect the function of their upper extremities. In particular, we introduce the design of a Mecanum-wheeled mobile robot, present its analysis, admittance control and passive path tracking control. We also integrate our platform with a virtual pick-and-place task and implement of virtual tunnels with assistive/resistive force fields along the desired path of the patient. Unlike the other therapeutic mobile devices that can only sustain passive and

resistive modes, the proposed holonomic mobile platform is an active rehabilitation device aimed for home therapy. Utilization of an active device is advantageous over its passive counterparts, since it allows for patients with limited upper limbs movements to be included in the robotic therapy program. Moreover, since the device can guide patients towards the clinically preferred movement patterns, it can improve accuracy of movement therapy and increase efficacy of rehabilitation protocols. The mobile platform can also be used as a measurement device, to characterize the range of motion and the isometric strength of the injured arm. Finally, the device can provide adaptive assistance to patients based on their task performance. Two versions of the holonomic mobile platform are implemented. In the first version, the robot is designed to have a symmetric structure and is equipped with a high fidelity force/torque sensor. The second prototype features series elastic actuation for backdriveability and is equipped with optical flow sensors to compensate for wheel slip during localization.

### 1.3 Contributions

- We have designed a novel self-aligning knee exoskeleton that allows translational movements of the knee joint on the sagittal plane along with the knee rotation.
  - Self-alignment feature guarantees perfect match between human joint axes and the device axes ensuring ergonomy and comfort throughout the therapy. This feature also significantly shortens the setup time required to attach the patient to the exoskeleton, allowing more effective time be spend on exercises instead of wasting it for adjustments.
- We have developed four conceptual designs for the knee exoskeleton based on different actuation and sensing principles: an impedance type concept, an admittance type concept with built-in force/torque sensing, a concept with series elastic actuation and a concept with variable stiffness actuation.
  - The impedance type concept relies on high-backdriveability and low apparent inertia of of the device to estimate output forces from applied motor torques, whereas the admittance type concept with built-in force/torque sensing uses sensor data to administer closed loop force control. The concept with series elastic actuation eliminates the need for costly force sensors, while the concept with variable stiffness actuation can control the mechanical stiffness of the end-effector independent from its configuration.
  - We have implemented the impedance type concept, derived its kinematic and dynamic models, and controlled the prototype un-

der open-loop impedance control. We have also experimentally characterized the performance of the knee exoskeleton and demonstrated ergonomics and usability of the device through human subject experiments.

- We have designed a novel Mecanum wheeled, admittance type, holonomic mobile rehabilitation robot for home therapy to administer table top exercises.
  - The choice of a mobile platform provides an unlimited planar workspace, while holonomic kinematics ensures that the robot can move/rotate independently on the plane to provide assistance to the patient.
- We have presented two different conceptual designs of holonomic mobile platform based on different actuation and sensing principles: an admittance type concept and a concept with series elastic actuation.
  - We have implemented the admittance type concept utilizing a force/torque sensor and synthesized an admittance controller for this design to ensure backdriveability under active control. We have integrated the admittance controller with virtual reality simulations and implemented virtual tunnels around nominal task trajectories such that the robot can impose assistive/resistive forces to the patient.
  - We have also implemented holonomic platform with series elastic actuation. The use of series elastic actuation eliminates the need for costly force sensors and enables implementation of closed loop

force control with higher controller gains, providing robustness against imperfections in the power transmission and allowing lower cost drive components to be utilized. This design is instrumented with optical flow sensors in addition to motor encoders, which enables (partial) compensation of the localization errors due to wheel slip.

- We have synthesized a passive velocity field controller (PVFC) for the holonomic platforms to provide assistance to the patients, such that the mobile platform follows a desired velocity field asymptotically while maintaining passivity with respect to external applied force/torque inputs.
  - PVFC is particularly suited for rehabilitation robotics, since this contour tracking controller ensures coordination and synchronization between various degrees of freedom, while letting patients to complete the task at their own preferred pace. Moreover, this method not only minimizes the contour error but also renders the closed loop system passive with respect to externally applied forces, ensuring coupled stability of the overall human-in-the-loop system.

## 1.4 Outline of the Thesis

The thesis is organized as follows. The design of rehabilitation robots for both upper and lower limb are discussed and design decisions are detailed in Chapter II. In particular, Section 2.1 discusses design criteria for rehabilitation robots for both upper and lower limbs, while Section 2.2 gives a brief explanation for the type selection of the robots. Section 2.3 discusses the conceptual designs developed based on different actuation and sensing principles. The kinematics of the robots are derived in Section 2.4 and the dynamic of the robots are modelled in Section 2.5. In Chapter III, the implementation of the robots are presented, detailing manufacturing methods and selection of sensors, actuators, and transmission elements. Chapter IV presents the controller synthesis for both robots, while the experimental characterization results are listed in Section 4.3. Chapter V concludes the thesis and gives a brief description of the planned future works, including clinical trials.

# Chapter II

## 2 Design of Rehabilitation Robots

In this chapter, we present the design of rehabilitation robots by introducing design criteria and detailing kinematic type selection. Several conceptual designs for the robots are presented, and kinematic and dynamic analysis are given.

### 2.1 Design Criteria

Following the terminology of Merlet [49], one can categorize the performance requirements of a mechanism into four distinct groups: Imperative requirements that must be satisfied for any design solution, optimal requirements for which a performance index must be maximized, primary requirements which take place in the specifications but can be relaxed to some extent to ensure a feasible solution, and secondary requirements which do not appear in the specifications but can be utilized to help decide among multiple solutions. Ensuring the safety and complying with the ergonomic needs of the patient are two imperative design requirements every rehabilitation robot must satisfy. Safety is typically assured by the selection of back-drivable actuation and power transmission, and with force/torque limits implemented in software, while predetermined ergonomic workspace volumes are imposed at the kinematic synthesis level. The absence of singularities in the workspace

is another imperative design requirement that ensures the forward and inverse kinematics of the robot can be solved uniquely at each point within the workspace. The optimal requirements for rehabilitation robots are generally imposed to improve kinematic isotropy and actuator utility. Specifically, to achieve high force bandwidths and a uniform “feel”, kinematic/dynamic isotropy and stiffness of the robot have to be maximized while its apparent inertia is being minimized.

A common primary requirement is the workspace volume index [49], the ratio between the workspace volume and the volume of the robot. Even though predetermined workspace volumes are generally imposed as imperative requirements, a large workspace volume index is still desired to reduce the collisions of the device with the operator or the environment. The footprint area is yet another primary requirement commonly imposed during design. Finally, the secondary requirements include low backlash, low-friction, high back-driveability, and low manufacturing costs. Friction, backlash, and backdriveability are mainly influenced by the selection of the actuators and the transmission, while choice of materials and link lengths may have an influence on manufacturing costs.

### **2.1.1 Lower Limb Rehabilitation Robot**

The imperative requirements for knee exoskeleton include safety and ergonomy since it is designed for robotic rehabilitation. In order to achieve safety, the knee robot should feature a backdriveable design to ensure safety even if power losses occur. The transmission ratio for the knee robot should be kept relatively low, not to severely effect backdriveability. To achieve ergonomy, exoskeleton should comfortably attach to patient. Moreover, for comfort-

able therapy sessions, the axes of rotation of the exoskeleton joints should perfectly correspond to the center of rotation of the knee. Knee is a complex joint whose center of rotation changes significantly in the sagittal plane during extension/flexion movements. Similar to other joints in human body, the center of rotation of the knee joint is also hard to locate, since the skin covers the joint. As a result, tracking the exact location of the center of knee joint by just observation is almost impossible. The joint misalignment can cause discomfort, pain and can even inflict injuries to the joint; therefore, sustaining joint alignment is another imperative design criteria to guarantee comfort and ergonomics.

The optimal design requirement of the knee exoskeleton is the singularity-free workspace of the robot. The workspace of the exoskeleton should cover all the translational and rotational movements of the knee joint for a large percentage of the population. Moreover, dexterity of the device within the workspace should be kept high. The primary requirements for the knee exoskeleton are symmetry of the workspace and the time it takes to wear the device. Ease of attachment/detachment of the exoskeleton is important to achieve efficient use of therapy time. Correspondingly, symmetric design is necessary to enable fast and easy calibration of the robot, regardless of the robot orientation.

The secondary requirements of the robot are low cost and low friction to minimize the effects of unmodelled device dynamics.

### **2.1.2 Upper Limb Rehabilitation Robot**

The imperative requirements for the upper limb rehabilitation robot are determined as safety, ergonomics and singularity free workspace. To sustain

safety, the robot should either be equipped with backdriveable actuation or safety should be actively imposed by force/torque control architectures. To ensure ergonomics and comfort, the upper limb rehabilitation robot should be designed to carry the weight of the human arm. Singularity free workspace is another imperative design requirement.

The optimal requirement for the upper limb rehabilitation robot is the workspace volume. The robot should cover all the useful range of motion of a healthy human.

The primary design requirements for the upper limb robot include low cost and small robot footprint. Moreover, since the robot is aimed to be used as a home therapy device, it should be available for large range of people with various budget limitations. In order to achieve a small footprint, the length of the robot should be kept just enough to place whole forearm and its width should be sufficient to embed mechanical and electronic components.

The secondary design requirements for the upper limb rehabilitation robot include low friction. The low friction is important to minimize the effects of unknown device dynamics.

## **2.2 Kinematic Type Selection**

This section details kinematic type selection for the lower limb and upper limb rehabilitation robots.

### **2.2.1 Lower Limb Rehabilitation Robot**

A 3-RRP mechanism is selected as the underlying kinematics for implementation of self-aligning knee joint, since this mechanism is capable of sustaining all necessary movements to cover the complex motion of the knee joint. In

particular, the 3-RRP planar parallel mechanism possesses three DoF, which include two translations in the plane and one rotation about the perpendicular axis. Thanks to its kinematic structure with close kinematic chains, the 3-RRP mechanism features high bandwidth and position accuracy, when compared with its serial counterparts. The 3-RRP mechanism is actuated with three grounded motors, and the torque of all three motors are combined to actuate rotation about the perpendicular axis. Hence, this mechanism allows high torques to be achieved for the knee by utilizing 3 lower torque actuators. Moreover, even though all three disks on the 3-RRP mechanism are aligned, the mechanism does not have any singularities within its workspace. The workspace of 3-RRP mechanism covers a large range of rotations, which is necessary for implementation of a knee joint whose rotation typically exceeds  $90^\circ$  during flexion and extension exercises.

### **2.2.2 Upper Limb Rehabilitation Robot**

The proposed upper limb rehabilitation device is an end-effector type robot. In particular, a holonomic mobile platform as shown in Figure 2.2 is selected as the underlying kinematics of the device. The holonomic mobile platform has an unlimited workspace; therefore, it can cover the whole range of motion of all patients. The footprint of the robot is designed so that the forearm and wrist can be conformably placed on the robot, relieving patients from the burden of supporting the weight of their own arm. The mobile robot is aimed to be used as a table top device and possesses three DoF, two translational DoF in plane and one rotational DoF, to sustain all possible planar movements. The mobile robot is chosen as of holonomic type, so that all of its DoF can be independently controlled. Although only three

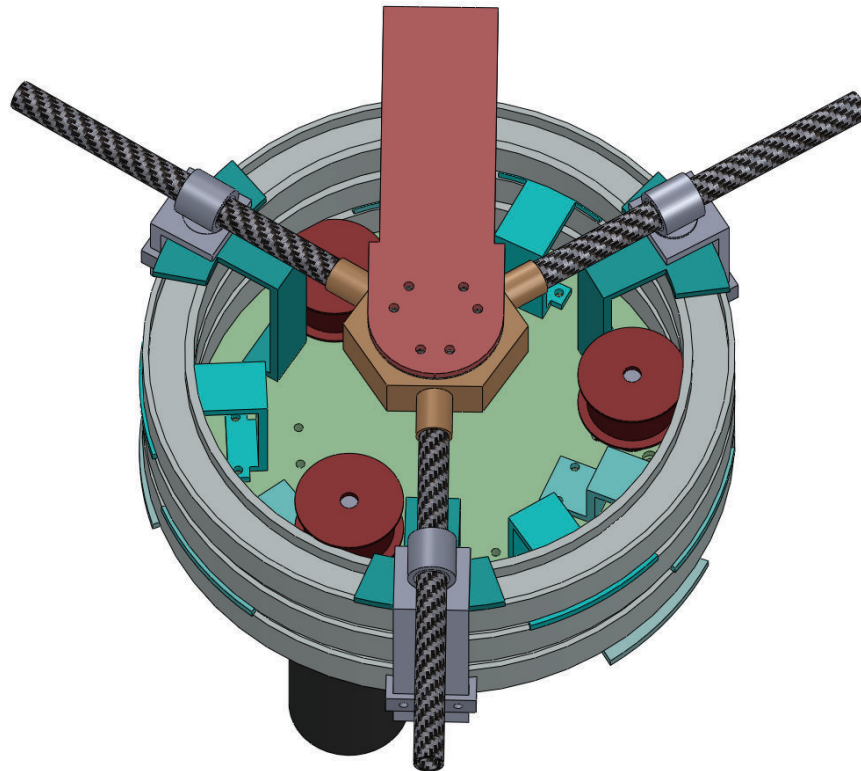


Figure 2.1: Kinematics of the knee rehabilitation robot is selected as a 3-RRP planar parallel mechanism.

actuators are sufficient to independently span all three DoF on a plane, the mobile platform is designed to use four actuators. Redundant actuation is preferred since it allows for lower power DC motors be utilized to achieve high forces/torques outputs at the task space of the robot. Furthermore, with a four wheeled design, the holonomic movement can be achieved using Mecanum wheels – omni-directional wheels with  $45^\circ$  angled rollers that can achieve enhanced traction and smoother motion. Evidence exist in literature that Mecanum wheeled robots can handle slipping better than three wheeled holonomic robot designs [50].

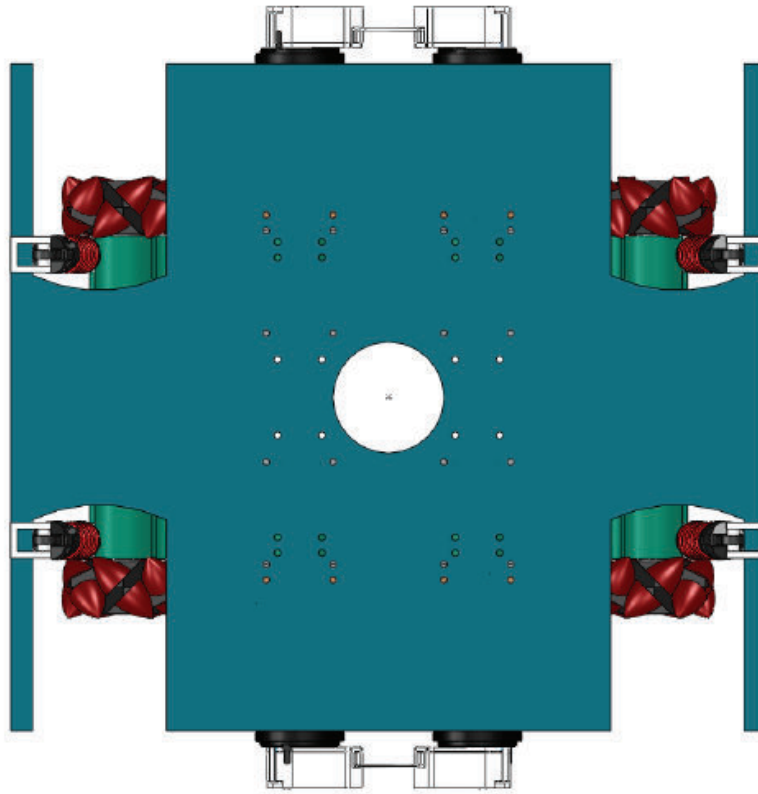


Figure 2.2: A holonomic mobile platform with Mecanum wheels is utilized to deliver table-top rehabilitation exercises.

### 2.3 Conceptual Designs

In this section, various conceptual designs for both upper limb and lower limb rehabilitation robots are presented. Specifically, four conceptual designs for the knee exoskeleton and two conceptual designs for the holonomic platform are described.

### 2.3.1 Knee Exoskeleton

#### Concept I: Impedance-Type Knee Exoskeleton

In the first design concept, actuation and transmission of the exoskeleton are selected to be backdriveable and the apparent inertia of the end effector is kept low such that the interaction forces with the patient can be controlled through open-loop impedance control. A sample design for impedance-type concept is depicted in Figure 2.3. In this design, the backdriveability of power transmission and low moving inertia not only enables high fidelity estimation of task space forces from motor torques, but also ensures safety even in case of a power loss. Moreover, impedance-type design features lower cost, since no force sensor are required to control interaction forces.

#### Concept II: Knee Exoskeleton with Embedded Force/Torque Sensing

Figure 2.4 presents a sample knee exoskeleton design with built in force/torque sensing. One way of achieving closed-loop force/impedance control is attaching a multi-axis force/torque (F/T) sensor to the robot end-effector. On the other hand, thanks to the kinematics of the knee exoskeleton, other low-cost solutions can also be implemented. Firstly, instead of utilizing a multi-axis F/T sensor, low-cost, single-axis force and torque cells can be embedded to the end-effector of the mechanism. One such implementation with three load cells (one of which is redundant) and one torque cell embedded in the design is depicted in Figure 2.4. Using the load cells attached to rigid links, the task space forces acting on the robot can be easily estimated by calculating the component of the force vector along each link, while the torque applied

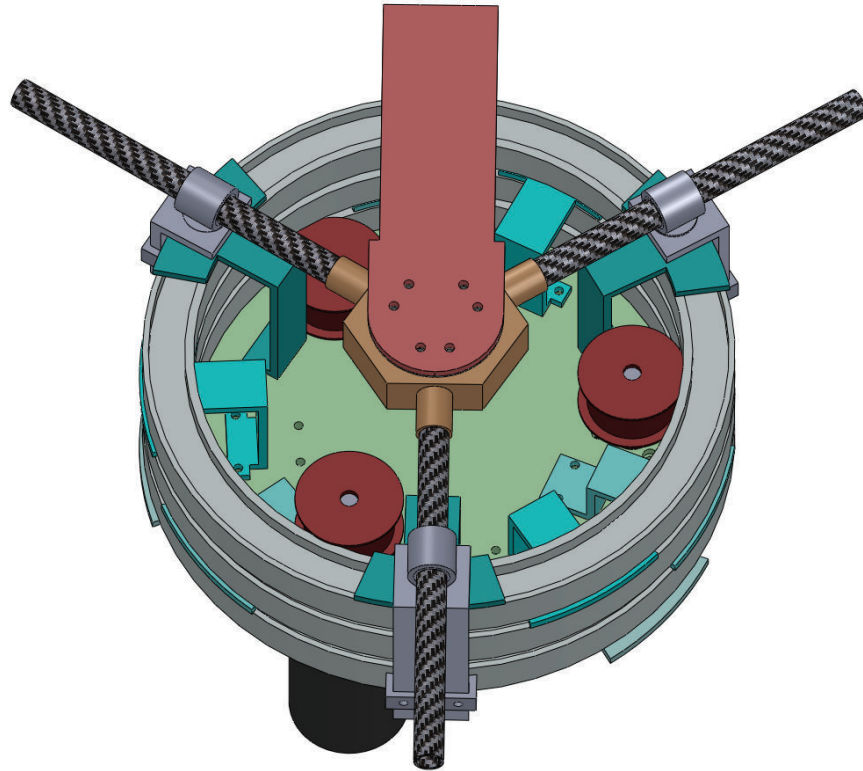


Figure 2.3: Solid model of an impedance-type 3-RRP knee exoskeleton.

to the the end effector can be measured directly using a torque cell.

### Concept III: Series Elastic Knee Exoskeleton

Figure 2.6 presents a conceptual design of the knee exoskeleton with Series Elastic Actuation (SEA). SEA is a relatively new concept that has emerged approximately 15 years ago [51]. SEA concept has benefited many fields of robotics such as, exoskeleton design! [52, 53], prosthetics [54, 55] and legged robot design [56, 57]. Control of interaction forces through series elastic actuation has certain advantages when compared to force control using force sensors. During explicit force control inherent non-collocation of the force

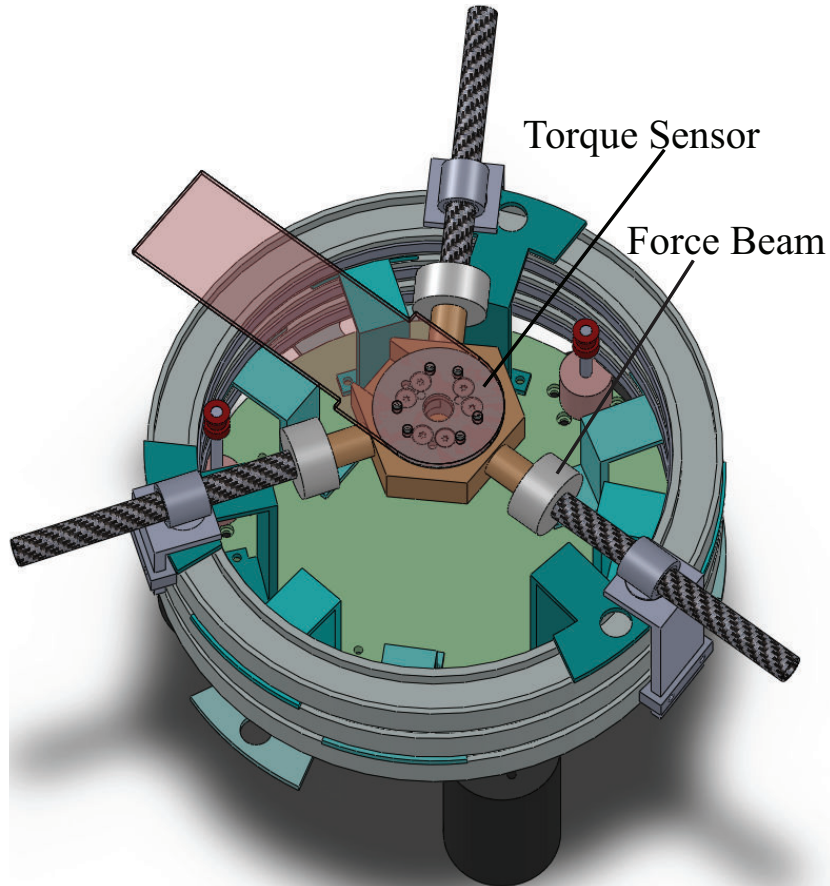


Figure 2.4: Knee exoskeleton with embedded force/torque sensing. Three load cells and a torque cell are built into the end effector to measure applied forces/torques.

sensor and the actuators (as shown in Figure 2.5) add additional dynamics to the system, negatively affecting the stability of the overall system [58]. In particular, non-collocation introduces an upper limit on the loop gain. Noting that the overall gain in the feedback loop is distributed between the force sensor and controller and given the fact that a typical force sensor has a stiffness in the order of  $10^7 N/m$ , the controller gains that cannot be set high during explicit force control to preserve stability. Hence, disturbance

rejection performance of explicit force controllers are typically very low. On the other hand SEAs have much smaller stiffness (on average  $10^3 - 10^4$  times lower than force sensors); therefore, systems utilizing SEA can implement much faster control loops. Since the control loop gains can be increased, resulting robustness allows lower cost actuators and transmission elements to be utilized during implementation. Moreover, since expensive force sensors can be replaced with digital position sensors while implementing SEAs and implementation of SEAs are of lower cost. In particular, compliant element of a SEA can be produced using low cost methods and materials, such as compliant mechanisms based on laser cut metal plates, and end effector forces can be determined by measuring the deflection of the compliant legs. However, due to intentionally added compliance, SEAs have limited bandwidth. Moreover, force estimates are highly dependent on the characterization of the stiffness of the compliant element.

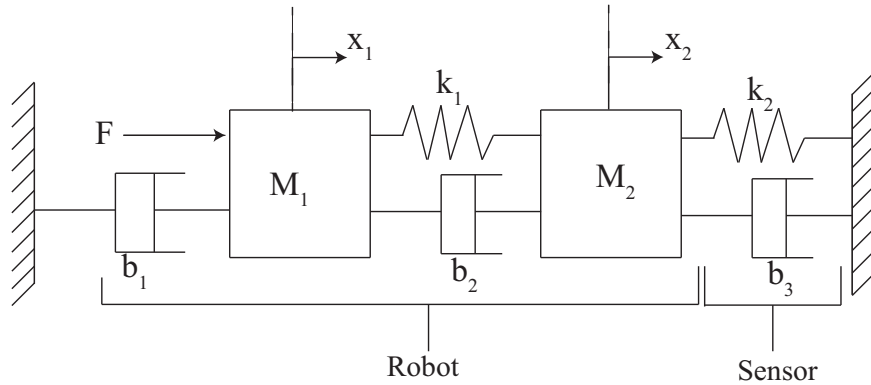


Figure 2.5: Inherent non-collocation between actuators and the force sensor reduces stability of the system.

In the SEA concept depicted in Figure 2.6, a compliant element is placed between the links and output of the 3-RRP mechanism and deflection of this compliant mechanism is measured as a low-cost means of obtaining the

forces and torques acting on the robot. In particular, the compliant body in Figure 2.6 is designed as a compliant 3-RRR mechanism, since this mechanism allows translations in plane and a rotation along the perpendicular axis. Therefore, by measuring the deflections of the compliant joints that are attached to the fixed base, it is possible to estimate all the forces and torques acting on the knee exoskeleton. In particular, the fixed frame of the compliant mechanism is attached to the rigid links and the output of the compliant joint is attached to the output of the 3-RRP mechanism. The joints of the compliant mechanism are designed as hinge-notch joints. The stiffness of the joints and the task space stiffness of the compliant mechanism are derived analytically as described in [59]. Independent joint displacements of the compliant mechanism can be measured using linear encoders and given the joint stiffness, end-effector forces/torques can be estimated. The range of the measured forces depends on the design of the compliant joint, while the force resolution of the system depends on the encoder resolution.

#### **Concept IV: Variable Impedance Knee Exoskeleton**

While adding compliance to an actuator, different levels of stiffness are required for various interactions: Precise position control tasks with good disturbance rejection characteristics require actuators with high stiffness, while impacts can be better regulated using actuators with low stiffness. Therefore, variable stiffness actuators (VSAs) have been introduced.

The most common approach to design of variable stiffness actuators is inspired from human muscles and utilizes antagonistic actuation. In one way of designing antagonistic actuators, two motors are connected to “spring like” compliant elements and these compliant elements are connected to the out-

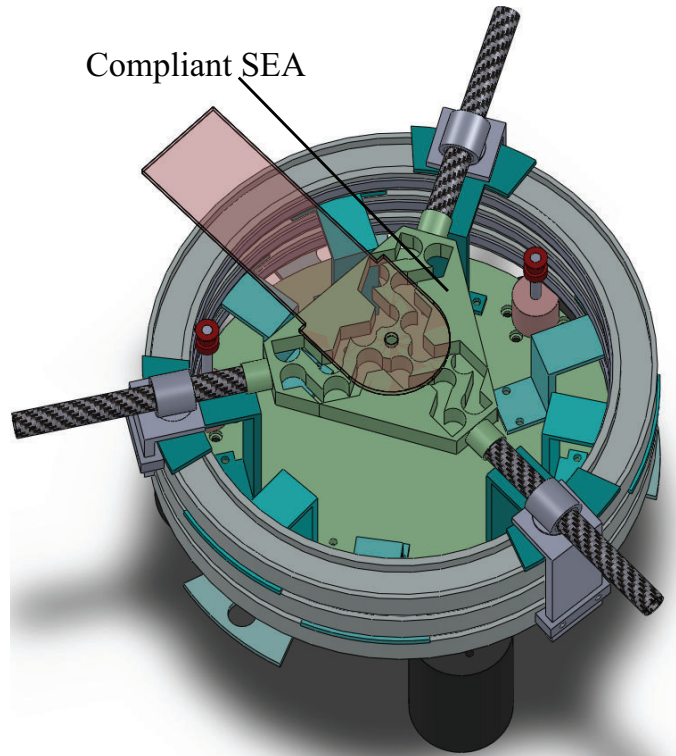


Figure 2.6: Knee exoskeleton with series elastic actuation. Deflections of the compliant mechanism attached to the end effector are measured to estimate forces/torques applied.

put link. The opposite movement of these two actuators creates compression forces on one element and tension on the other. It has been shown in literature that if the force function of the springs are non-linear (in particular, if it is quadratic), this conjugate actuator movement does not affect the configuration of the output link position but changes its stiffness [60]. Similarly, if both actuators move in the same direction, the configuration of the output link is changed preserving its stiffness.

Implementation of variable stiffness actuators with the antagonistic approach have been studied by several groups. In particular, in [61] Bicchi *et al.* proposed a VSA actuator based on McKibben artificial muscles and

further developed it in [62]. In [63], Migliore *et al.* introduced use of curvature surfaces to create nonlinear spring elements. In [64], Yamaguchi *et al.* implemented antagonistic joints in biped locomotion [64], while bidirectional antagonistic joints were utilized by DLR in [65]. Figure 2.7 depicts one sam-

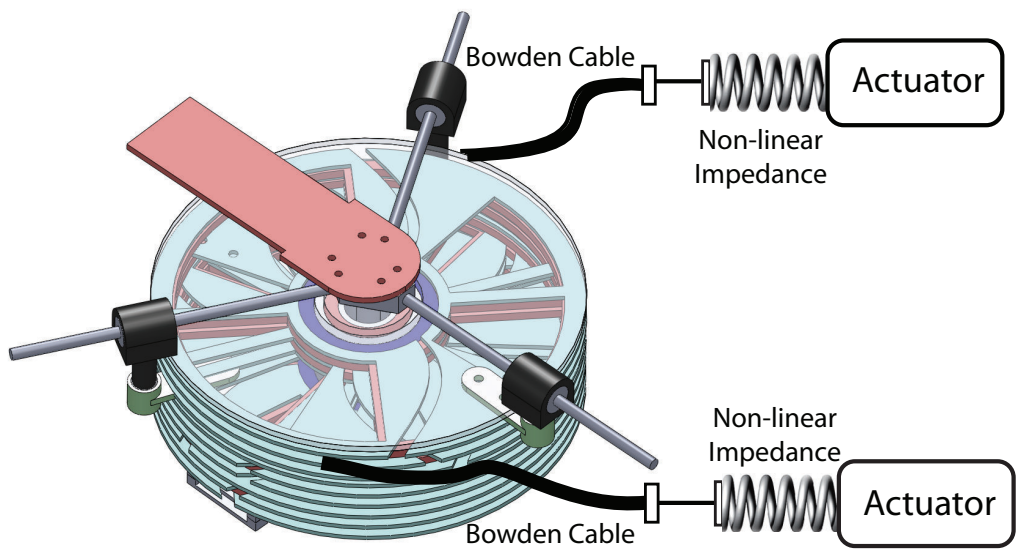


Figure 2.7: Knee exoskeleton with variable impedance antagonist actuation.

ple implementation of the variable impedance actuation for the self-aligning joint mechanism. In this design, each of the three disks is composed of a combination of sub-disks with special edges. The inner slots on the disks are used for the attachment of two Bowden cables. Bowden cables are working according to the antagonist principle and each cable can pull the disk up to  $180^\circ$ . Bowden cables are attached to non-linear springs (or more generally impedances) to enable mechanical variable impedance actuation.

### 2.3.2 Holonomic Mobile Platform

Two conceptual designs are considered for the holonomic mobile platform. The first design embeds a multi-axis force/torque sensor, while the second one is based on series elastic actuation.

#### **Concept I: Holonomic Mobile Platform with Force/Torque Sensor**

The first conceptual design of the holonomic mobile platform is based on a multi-axis force/torque sensor as shown in Figure 2.8. The force sensor is used to achieve backdriveability of the platform under active control. In particular, explicit force (admittance) controllers can be implemented to ensure the robot render desired forces to the patient. The proposed design has symmetric actuator configurations. The robot uses motor encoders as position sensors and a high fidelity force/torque sensor which is attached to the robot from the kinematic center of the robot. The robot has shock spring damper system to ensure contact of each wheel to the ground. Thanks to the Mecanum wheels the robot can move and rotate independently in plane. Unlike holonomic robots with omni wheels, Mecanum wheeled holonomic robots uses four actuated wheels instead of three and the extra motor power increases the task space forces that robot can render.

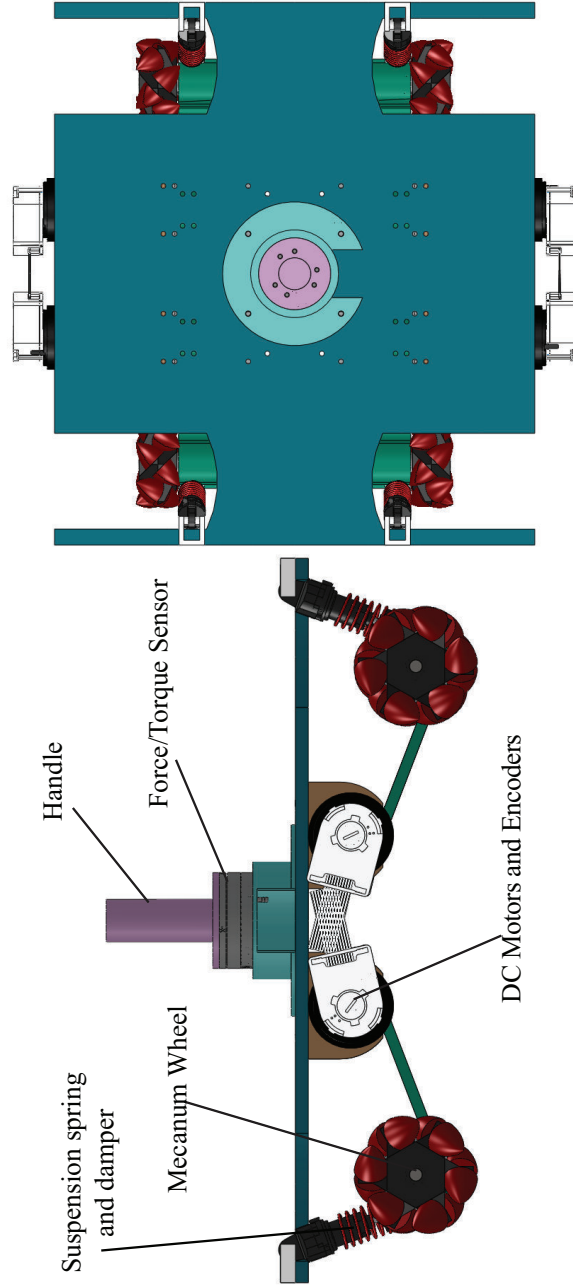


Figure 2.8: The holonomic mobile platform can be utilized with a multi axis force/torque sensor and symmetric actuation.

## **Concept II: Holonomic Mobile Platform with Series Elastic Actuation**

The second conceptual design of the holonomic mobile platform utilizes SEA instead of a multi-axis force/torque sensor. SEA not only allows for high-fidelity estimation of interaction forces, but also allows for the use of lower cost actuator and transmission components, thanks to higher controller gains. As a result, the holonomic mobile platform with series elastic actuation has much lower cost than the concept based on a multi-axis force sensor. Thanks to its asymmetric actuator orientations, this concept has smaller dimensions. This concept is also equipped with optical flow sensors to compensate for the position errors due wheel slip, resulting in better local position estimation.

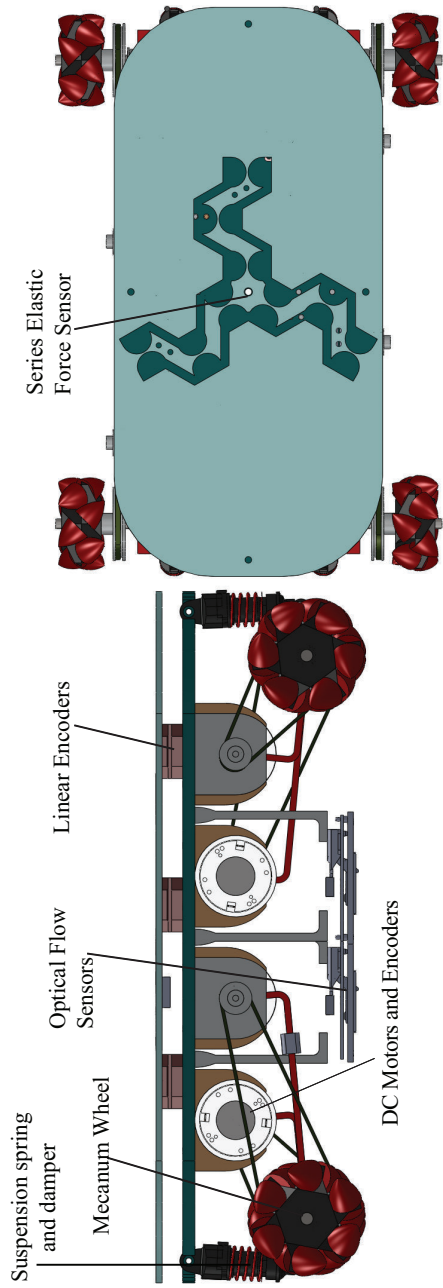


Figure 2.9: The design of holonomic mobile platform with series elastic actuation and asymmetric motor configuration.

## 2.4 Kinematics

In this section, the forward and inverse kinematics of the knee exoskeleton and the holonomic mobile platform are derived analytically.

### 2.4.1 Kinematics of the Knee Exoskeleton

Both forward and inverse kinematics of the robot are derived at configuration and motion levels, respectively.

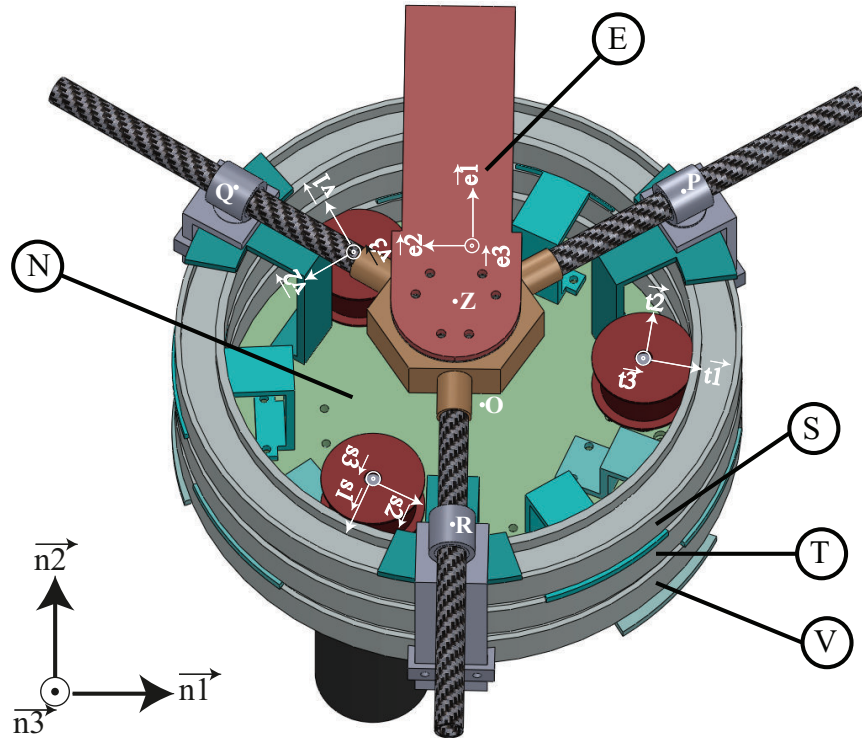


Figure 2.10: Solid model of the 3-RRP mechanism. Bodies, points, basis vectors and variables used in kinematic analysis are marked on the figure.

The 3-RRP mechanism consists of five rigid bodies  $N, S, T, V$  and  $E$ . In Figure 2.10, the point  $Z$  is fixed in  $E$ , point  $Q$  is fixed in body  $S$ , point  $P$  is fixed in body  $T$ , point  $R$  is fixed in body  $V$  and point  $O$  is fixed in body  $N$ .

Body  $N$  represents the fixed frame, bodies  $S$ ,  $T$  and  $V$  have simple rotations about point  $O$  with revolute joints and attached to the moving platform  $E$  through revolute and prismatic joints which are collocated at points  $P$ ,  $Q$  and  $R$ , respectively. The common out of the plane unit vector is denoted by  $\vec{n}_3$  and basis vectors of each body are indicated in Figure 2.10.

Dimensions of the mechanism are defined as follows: The fixed distance  $OP$  is defined as  $l_1$ ,  $OQ$  is defined as  $l_2$  and  $OR$  is defined as  $l_3$ , while the distance  $ZP$  is defined as  $s_1$ ,  $ZQ$  is defined as  $s_2$  and  $ZR$  is defined as  $s_3$ . The angle between the line  $\vec{n}_1$  and  $\vec{t}_1$  vector is  $Cq_1$ , the angle between  $\vec{n}_1$  and  $\vec{s}_1$  is  $Cq_2$  and the angle between  $\vec{n}_1$  and  $\vec{v}_1$  is  $Cq_3$  where  $C$  is the transmission ratio. All angles are positive when measured counter clockwise.

The inputs to the mechanism are set as the angles  $q_1$ ,  $q_2$  and  $q_3$  (i.e. the links  $S$ ,  $T$  and  $V$  are actuated) and their time derivatives. At the initial configuration  $\vec{e}_1$  vector is parallel to  $\vec{n}_1$ . The output of the system is defined as the position of the end effector point  $Z$ , when measured from the fixed point  $O$  and the orientation of body  $E$ , measured with respect to body  $N$ . In particular, the scalar variables for outputs are defined as  $x = r^{OZ}\vec{n}_1$ ,  $y = r^{OZ}\vec{n}_2$ , and  $\theta = \text{atan2}\left(\frac{\vec{e}_2 \cdot \vec{n}_2}{\vec{e}_2 \cdot \vec{n}_1}\right)$ , where  $r^{OZ}$  is the distance between points  $O$  and  $Z$ .

### Configuration Level Kinematics

To ease calculations, three auxiliary reference frames, namely  $K$ ,  $L$  and  $M$  are defined such that  $\vec{k}_1$  extends from  $Z$  to  $P$ ,  $\vec{l}_1$  extends from  $Z$  to  $S$  and  $\vec{m}_1$  extends from  $Z$  to  $R$ , while  $\vec{k}_3 = \vec{l}_3 = \vec{m}_3 = \vec{n}_3$ . Using the auxiliary reference frames, the vector loop equations that govern the geometry of the

mechanism can be expressed as

$$x \cdot \vec{n}_1 + y \cdot \vec{n}_2 + s_1 \cdot \vec{k}_1 - l_1 \cdot \vec{t}_1 = \vec{0} \quad (1)$$

$$x \cdot \vec{n}_1 + y \cdot \vec{n}_2 + s_2 \cdot \vec{l}_1 - l_2 \cdot \vec{s}_1 = \vec{0} \quad (2)$$

$$x \cdot \vec{n}_1 + y \cdot \vec{n}_2 + s_3 \cdot \vec{m}_1 - l_3 \cdot \vec{v}_1 = \vec{0} \quad (3)$$

Expressing the vector loops in one of the frames (typically in  $N$ ), these vector equations yield 6 independent scalar equations, which form the base for solution of configuration level kinematics.

### Configuration Level Forward Kinematics

Three vector equations that are derived in the previous subsection yield to six nonlinear scalar equations with six unknowns. Given  $q_1$ ,  $q_2$  and  $q_3$ , solving these nonlinear equations analytically for  $x$ ,  $y$  and  $\theta$  (and intermediate variables  $s_1$ ,  $s_2$  and  $s_3$ ) yields

$$x = -\frac{M}{\sqrt{3}(K^2 + L^2)} \quad (4)$$

$$y = c_{22} - \frac{K}{L}c_{21} - \frac{KM}{\sqrt{3}L(K^2 + L^2)} \quad (5)$$

$$\theta = \tan^{-1}\left(\frac{K}{L}\right) \quad (6)$$

where

$$\begin{aligned}
K &= c_{12} + c_{32} + \sqrt{3}c_{31} - 2c_{22} - \sqrt{3}c_{11} \\
L &= c_{11} + c_{31} + \sqrt{3}c_{12} - 2c_{21} - \sqrt{3}c_{32} \\
M &= L(L - \sqrt{3}K)c_{12} - L(K + \sqrt{3}L)c_{11} \\
&\quad - (L - \sqrt{3}K)(Lc_{22} - Kc_{21})
\end{aligned}$$

and

$$\begin{aligned}
c_{11} &= l_1 \cos(q_1), c_{12} = l_1 \sin(q_1) \\
c_{21} &= l_2 \cos(q_2), c_{22} = l_2 \sin(q_2) \\
c_{31} &= l_3 \cos(q_3), c_{32} = l_3 \sin(q_3)
\end{aligned}$$

### Configuration Level Inverse Kinematics

Given  $x$ ,  $y$  and  $\theta$ , the inverse kinematics problem can be solved analytically for joint positions  $q_1$ ,  $q_2$  and  $q_3$  by using the vector cross product method suggested by Chace [66] as

$$q_1 = \tan^{-1}\left(\frac{M_1}{L_1}\right) \quad (7)$$

$$q_2 = \tan^{-1}\left(\frac{M_2}{L_2}\right) \quad (8)$$

$$q_3 = \tan^{-1}\left(\frac{M_3}{L_3}\right) \quad (9)$$

where

$$\begin{aligned}
K_1 &= x \sin(\theta + \frac{\pi}{3}) - y \cos(\theta + \frac{\pi}{3}) \\
K_2 &= x \sin(\theta + \pi) - y \cos(\theta + \pi) \\
K_3 &= x \sin(\theta - \frac{\pi}{3}) - y \cos(\theta - \frac{\pi}{3}) \\
M_1 &= K_1 \cos(\theta + \frac{\pi}{3}) - \sqrt{l_1^2 - K_1^2} \sin(\theta + \frac{\pi}{3}) \\
L_1 &= -K_1 \sin(\theta + \frac{\pi}{3}) - \sqrt{l_1^2 - K_1^2} \cos(\theta + \frac{\pi}{3}) \\
M_2 &= K_2 \cos(\theta + \pi) - \sqrt{l_2^2 - K_2^2} \sin(\theta + \pi) \\
L_2 &= -K_2 \sin(\theta + \pi) - \sqrt{l_2^2 - K_2^2} \cos(\theta + \pi) \\
M_3 &= K_3 \cos(\theta - \frac{\pi}{3}) - \sqrt{l_3^2 - K_3^2} \sin(\theta - \frac{\pi}{3}) \\
L_3 &= -K_3 \sin(\theta - \frac{\pi}{3}) - \sqrt{l_3^2 - K_3^2} \cos(\theta - \frac{\pi}{3})
\end{aligned}$$

### Motion Level Kinematics

Motion level kinematic equations are derived by taking the time derivative of the vector loop equations derived configuration level kinematics. Six independent scalar equations can be obtained by projecting the vector equations onto the  $\vec{n}_1$  and  $\vec{n}_2$  unit vectors.

### Motion Level Forward Kinematics

Given actuator velocities  $\dot{q}_1$ ,  $\dot{q}_2$  and  $\dot{q}_3$ , motion level forward kinematics problem can be solved for end-effector velocities  $\dot{x}$ ,  $\dot{y}$  and  $\dot{\theta}$  (along with intermediate variables  $\dot{s}_1$ ,  $\dot{s}_2$  and  $\dot{s}_3$ ) as

$$\dot{X}_1 = A_1^{-1} B_1 \tag{10}$$

where

$$A_1 = \begin{pmatrix} 1 & 0 & -s_1 \sin(\theta + \frac{\pi}{3}) & \cos(\theta + \frac{\pi}{3}) & 0 & 0 \\ 0 & 1 & s_1 \cos(\theta + \frac{\pi}{3}) & \sin(\theta + \frac{\pi}{3}) & 0 & 0 \\ 1 & 0 & -s_2 \sin(\theta + \pi) & 0 & \cos(\theta + \pi) & 0 \\ 0 & 1 & s_2 \cos(\theta + \pi) & 0 & \sin(\theta + \pi) & 0 \\ 1 & 0 & -s_3 \sin(\theta - \frac{\pi}{3}) & 0 & 0 & \cos(\theta - \frac{\pi}{3}) \\ 0 & 1 & s_3 \cos(\theta - \frac{\pi}{3}) & 0 & 0 & \sin(\theta - \frac{\pi}{3}) \end{pmatrix}$$

while

$$\dot{X}_1 = \begin{pmatrix} \dot{x} \\ \dot{y} \\ \dot{\theta} \\ \dot{s}_1 \\ \dot{s}_2 \\ \dot{s}_3 \end{pmatrix} \quad \text{and} \quad B_1 = \begin{pmatrix} -l_1 \dot{q}_1 \sin(q_1) \\ l_1 \dot{q}_1 \cos(q_1) \\ -l_2 \dot{q}_2 \sin(q_2) \\ l_2 \dot{q}_2 \cos(q_2) \\ -l_3 \dot{q}_3 \sin(q_3) \\ l_3 \dot{q}_3 \cos(q_3) \end{pmatrix}$$

### Motion Level Inverse Kinematics

Given solution the motion level forward kinematics

For a motion level inverse kinematics problem end-effector velocities  $\dot{x}$ ,  $\dot{y}$ ,  $\dot{\theta}$  are given and it is expected to solve for actuator velocities  $\dot{q}_1, \dot{q}_2, \dot{q}_3$  (and optionally  $\dot{s}_1, \dot{s}_2, \dot{s}_3$ ). Again using the derived six linear equations six unknowns are called for solution. Similarly problem is solved by matrix

calculation:

$$A_2 \dot{X}_2 = B_2$$

$$\dot{X}_2 = A_2^{-1} B_2$$

The motion level inverse kinematics of the 3-RRP mechanism can easily be found, once the motion level forward kinematics problem is solved, by simply taking the inverse of  $A_1$  matrix derived in Equation 2.4.1.

### 2.4.2 Kinematics of the Holonomic Mobile Platform

The mobile robot presented in this study has three degrees of freedom in its task space. On the other hand, the robot uses four wheels and their corresponding actuators to sustain motions in the task space; therefore, the mobile device is a redundant mechanism.

Figure 2.11 depicts the CAD model of the holonomic mobile platform, on which important points, bodies and frames are marked. In particular,  $N$  represents the Newtonian reference frames,  $H$  denotes the holonomic platform,  $W_i$  ( $i=1,\dots,4$ ) are the wheels, while  $S_i$  ( $i=1,\dots,4$ ) denote the frames attached to the rollers of the Mecanum wheels.  $H_o$  marks the geometric center of the robot, while  $L$  is the vertical and  $T$  is the horizontal distance from  $H_o$  to the geometric center of the wheels  $W_{io}$ , respectively.

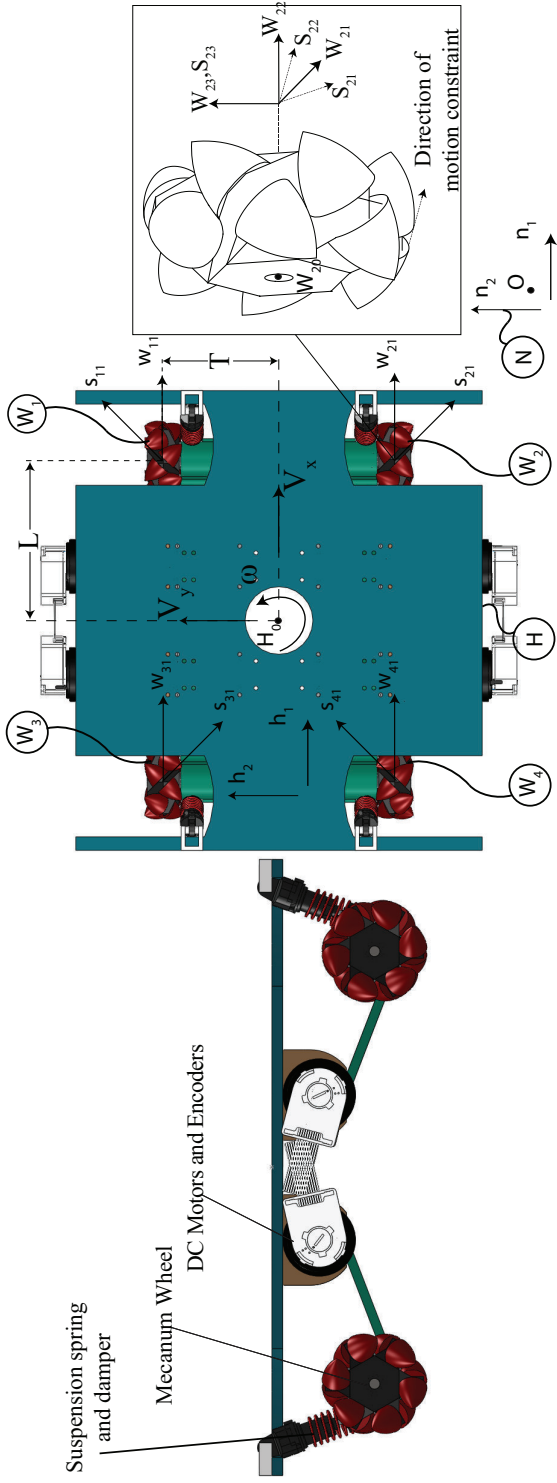


Figure 2.11: Solid model of the Mecanum-wheeled mobile platform on which important points, bodies and frames are marked.

Let the velocity of the geometric center of the robot  $H_o$  with respect to the ground  $N$  be defined as

$${}^N\vec{V}^H = V_x\vec{n}_1 + V_y\vec{n}_2 \quad (11)$$

where  $V_x$  and  $V_y$  represent the magnitude of the velocities along  $\vec{n}_1$  and  $\vec{n}_2$  directions; and let the angular velocity of the robot with respect to the ground be defined as

$${}^N\vec{\omega}^H = \omega\vec{n}_3 \quad (12)$$

where  $\omega$  denotes the magnitude of the angular velocity. Given the angular velocity of each wheel  $W_i$  with respect to the robot base  $H$  as

$${}^H\vec{\omega}^{W_i} = \dot{\theta}_i\vec{\omega}_{i2} \quad \text{for } i=1,\dots,4 \quad (13)$$

where  $\dot{\theta}_i$  is the magnitude of angular velocity of each wheel, the velocity of the center of the rollers  $S_{i_o}$  in contact with the ground can be derived as

$${}^N\vec{V}^{S_{i_o}} = {}^N\vec{V}^{H_o} + {}^N\vec{\omega}^H \times \vec{r}^{H_oW_{i_o}} + {}^H\vec{\omega}^{W_i} \times \vec{r}^{W_{i_o}S_{i_o}} \quad (14)$$

where  $\vec{r}^{H_oW_{i_o}}$  is the position vector from the center of robot to the center of each wheel and  $\vec{r}^{W_{i_o}S_{i_o}}$  is the position vector from wheel center to contacting roller center for each wheel. Assuming the rollers in contact with the ground cannot slip sideways, the  $\vec{s}_{i2}$  components of the velocities  ${}^N\vec{V}^{S_{i_o}}$  are set to zero as holonomic constraints restricting the motion of the robot as

$${}^N\vec{V}^{S_{i_o}} \cdot \vec{s}_{i2} = 0 \quad \text{for } i=1,\dots,4 \quad (15)$$

velocity of the contact point of rollers with respect to rollers centers are zero. Therefore, the velocity of the contact point of each wheel,  $P_i$ , can be written as;

$$\sum_{i=1}^4 {}^N\vec{V}^{P_i} = \sum_{i=1}^4 {}^N\vec{V}^{S_i} \quad (16)$$

The rollers are modeled as purely rolling bodies; therefore, sliding is neglected. For each of the contacting rollers two constraint equations can be written.

$$\begin{aligned} {}^N\vec{V}^{P_i} \cdot \vec{W}_{i3} &= 0 \\ {}^N\vec{V}^{P_i} \cdot \vec{s}_{i3} &= 0 \end{aligned} \quad (17)$$

Given these holonomic constraints, motion level inverse kinematics of the mobile platform can be derived as

$$\begin{bmatrix} \dot{\theta}_1 \\ \dot{\theta}_2 \\ \dot{\theta}_3 \\ \dot{\theta}_4 \end{bmatrix} = J^{-1} \begin{bmatrix} Vx \\ Vy \\ \omega \end{bmatrix} \quad (18)$$

with inverse Jacobian matrix  $J^{-1}$

$$J^{-1} = \frac{1}{R} \begin{bmatrix} 1 & -1 & -(L+T) \\ 1 & 1 & (L+T) \\ 1 & 1 & -(L+T) \\ 1 & -1 & (L+T) \end{bmatrix} \quad (19)$$

where  $R$  denotes the radius of the wheels. Due to redundant actuation of the robot, a solution to the motion level forward kinematics of the mobile platform can be derived by taking the Moore-Penrose inverse of the Jacobian

matrix as

$$J^\dagger = (J^T \times J)^{-1} \times J^T \quad (20)$$

Then the velocity level forward kinematics matrix is derived as,

$$J^\dagger = \begin{vmatrix} 1 & 1 & 1 & 1 \\ -1 & 1 & 1 & -1 \\ -\frac{1}{L+R} & \frac{1}{L+R} & -\frac{1}{L+R} & \frac{1}{L+R} \end{vmatrix} \quad (21)$$

The derivation of the Jacobian and inverse Jacobian matrices are explained in detail in [67].

## 2.5 Dynamics

### 2.5.1 Dynamics of the Knee Exoskeleton

The dynamic equations of knee exoskeleton is derived using Kane's method [68]. The external forces/torques acting on the robot occur as a result of knee-robot interaction namely,  $F_x$ ,  $F_y$ ,  $\tau_z$  and the motor torques  $\tau_i$  which are actuating the input links. The actuated joints and the task space velocities are used to select generalized speeds. Acceleration level kinematics of the device is derived and partial velocities of the mass centers and force acting points are formed in order to implement Kane's method. Inertia of each moving parts of the robot is estimated using its CAD model. The equations of motion of the robot are derived symbolically using computational techniques and task space inertia, gravity and Coriolis terms are derived.

### 2.5.2 Dynamics of the Mobile Platform

The dynamic equations governing the motion of the mobile robot is also derived using Kane's method [68]. The external forces/torques acting on the robot are identified as the human forces  $F_x$ ,  $F_y$  and torque  $\tau_z$  at the end effector and the motor torques  $\tau_i$  at each wheel. Moreover, since wheels are likely to slip along  $\vec{w}_{i1}$  direction while the rollers may slip along  $\vec{s}_{i1}$  direction, two distinct velocity dependent friction forces are considered to act at the contact points of the rollers with the ground. If the wheels and rollers are assumed not to slip, these forces drop from the resulting equations of motion, since they chase to do work. To implement Kane's method, acceleration level kinematics of the device is derived and partial velocities of the mass centers and force acting points are formed. Inertia of each component of the robot is estimated using its CAD model. Finally, the equations of motion of the robot are derived symbolically and task space inertia and Coriolis matrices are determined.

# Chapter III

## 3 Implementation

This chapter presents the implementation details for prototypes of the knee exoskeleton and the holonomic mobile platform.

### 3.1 Implementation of the Knee Exoskeleton

Figure 3.1 depicts the prototype of Concept I, impedance-type knee exoskeleton. In the figure, the output link of the robot, which connects the robot to the lower leg, and the ground link, which is directly connected to upper leg, are removed for a less occluded view of the mechanism. The complete assembly of the exoskeleton, attached to a human subject is presented Figure 3.2.

The rings of the robot are manufactured from aluminum and each ring is supported with three auxiliary parts with three ball shaped teflon rollers. Belt drive transmission is utilized to transfer power from direct drive motors to the rings. In the current implementation, the transmission ratio is set to 5.6. The belts are placed inside the rings, such that the actuators of the robot can be located inside the rings, decreasing mechanism footprint.

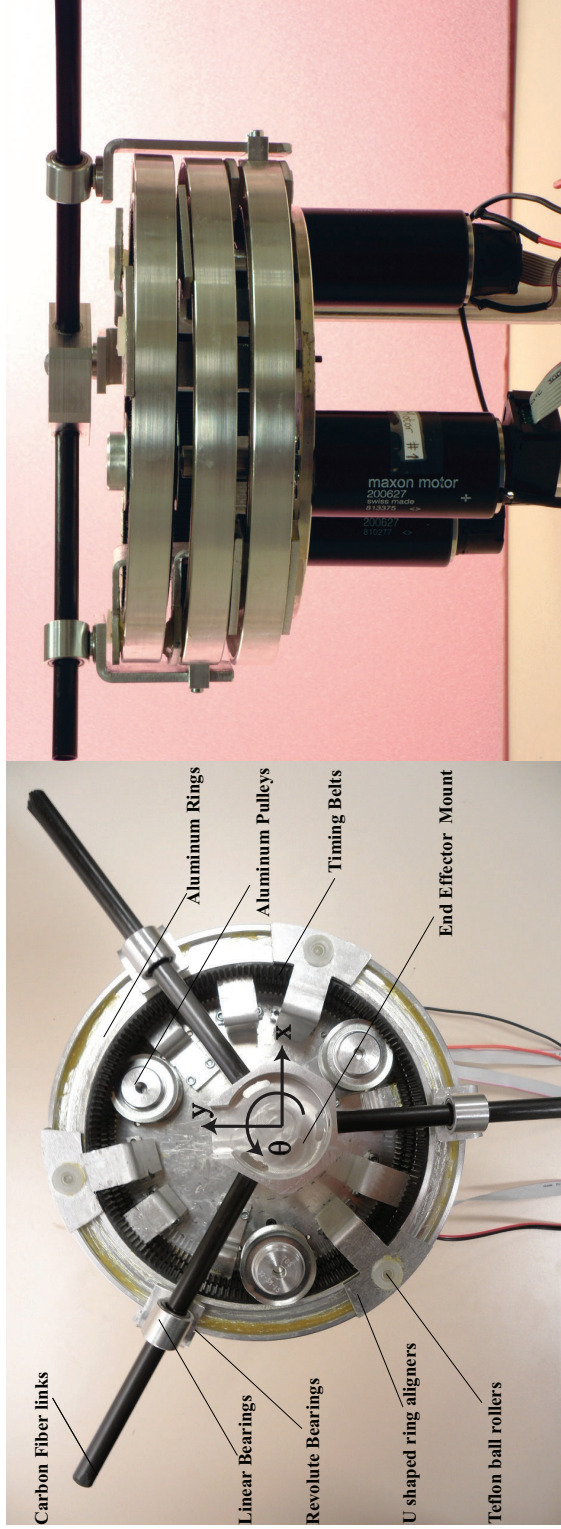


Figure 3.1: The knee robot is built using three concentric rings that are driven internally using a belt drive transmission. The rings are supported and aligned using custom brackets manufactured from aluminum and teflon ball rollers.

In contrast to direct drive actuation, belt drive provides torque amplification while simultaneously enabling concentric placement of the three rings. Belt drives are preferred due to their low cost and widespread availability in various sizes and properties. The movements of the rings are transferred to an upper planar plane by using aluminum links and these aluminum links are merged with carbon fiber tubes via concentric revolute and prismatic joints. Finally, the carbon fiber tubes, that enable a low weight and high stiffness implementing of the end-effector, are connected to the end effector of the robot with  $120^\circ$  angle between each tube. The exoskeleton is actuated using direct-drive graphite-brushed DC motors that possess 180 mNm continuous torque output. The direct drive actuators are preferred since they are highly back-driveable. Optical encoders attached to the motors have a resolution of 2000 counts per revolution, under quadrature decoding. The robot is designed to feature a symmetric structure, such that it possesses high kinematic isotropy and can be applied to both left and right knees. The first prototype of the robot has a large translational workspace, covering up to 180 mm translations along  $x$  and  $y$  axes. The exoskeleton can also sustain infinite rotations about the perpendicular axis.

## **3.2 Implementation of the Holonomic Platform**

Both Concept I and Concept II are implemented for the holonomic mobile platform. This section details both implementations.

### **3.2.1 Concept I: Holonomic Platform with F/T Sensor**

The holonomic movement with the Mecanum wheels is achieved by installing four wheels in a special order such that the rollers of first and fourth wheels



Figure 3.2: The isometric view of the exoskeleton prototype attached to knee.

and rollers of second and third wheels possess a  $90^\circ$  orientation difference about the vertical axis. Since the robot is equipped with four wheels, the design integrates a suspension system to ensure that all wheels are in contact with the ground at all times. Specifically, the suspension springs are chosen among the commercial suspension components for RC cars and have  $10\text{mm}$  stroke. The connection parts and upper body of the robot are manufactured from aluminum. The actuators of the robot are chosen as brushed DC motors with  $180\text{mNm}$  continuous torques. Belt driven transmission, with a torque amplification gain of 3.5, is used for robot actuation. The robot has dimensions of  $340\text{mm} \times 300\text{mm} \times 85\text{mm}$  and weights approximately 5kg.

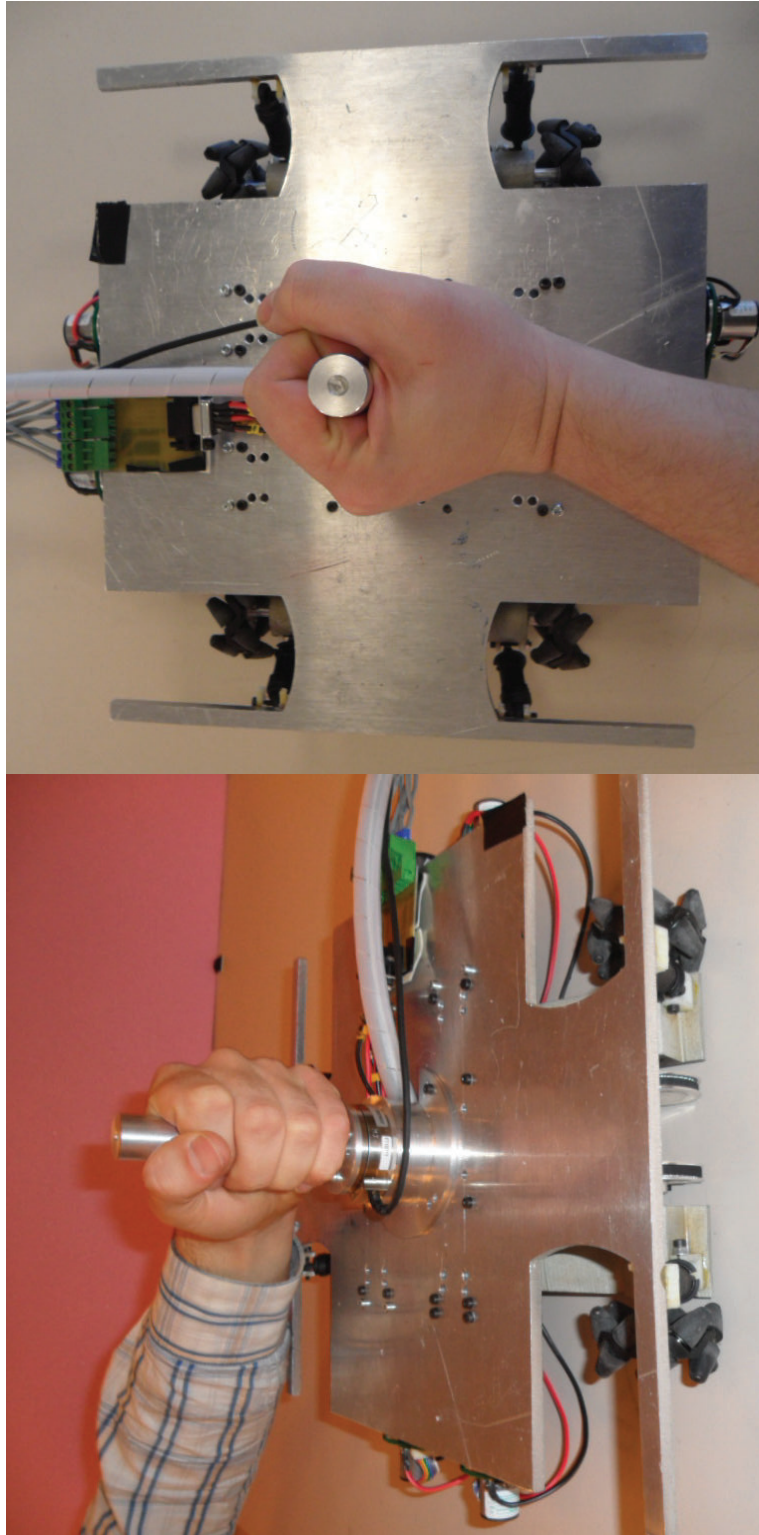


Figure 3.3: Concept I: Holonomic mobile platform with multi-axis force/torque sensor

The configuration of the robot is estimated through dead reckoning based on 15bit encoders located at the motor axes. Even though the actuators are back-driveable, the mobile robot is not, due to the constraints imposed by Mecanum wheels. Therefore, the robot is equipped with a force sensor so that back-driveability can be achieved through active control. In the current prototype, a six DoF sensor is used such that all the forces/torques applied by the patient can be evaluated to better guide to the patient.

Figure 3.3 presents the prototype of Concept I. Note that, this prototype is implemented to evaluate the feasibility of the holonomic robot as a rehabilitation device and to study its effectiveness for practical rehabilitation tasks. Hence, laboratory-grade high accuracy components are used in this prototype without much consideration of their cost.

### **3.2.2 Concept II: Holonomic Platform with SEA**

As a second prototype, Concept II – holonomic mobile platform with SEA, is implemented. This prototype address several problems that were identified after the implementation of Concept I: i) large device footprint, ii) poor localization performance under wheel slip, and iii) high-cost. In particular, due to its symmetric design the first prototype has a large volume. Multi-axis force torque sensor drastically increases the device cost. Localization solely based in motor encoders is subject to high drift, errors due to slipping can not be fully neglected. Moreover, since the robot kinematics are calculated in the motion level, configuration of the robot can only be obtained via numeric integration of its velocities. Noise is amplified during numerical differentiation and drift is introduced during integration.

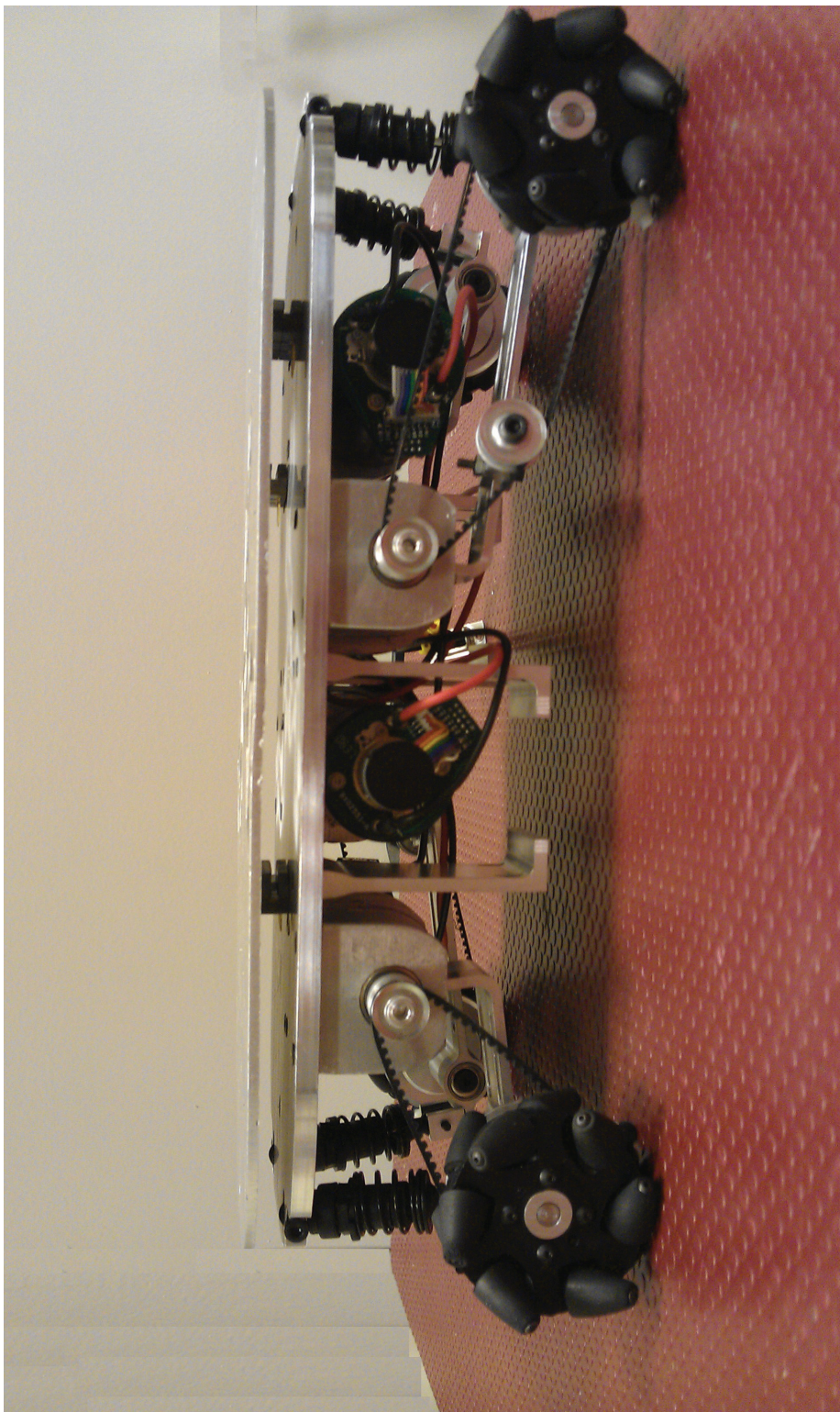


Figure 3.4: Top view of the holonomic mobile platform with series elastic actuation.

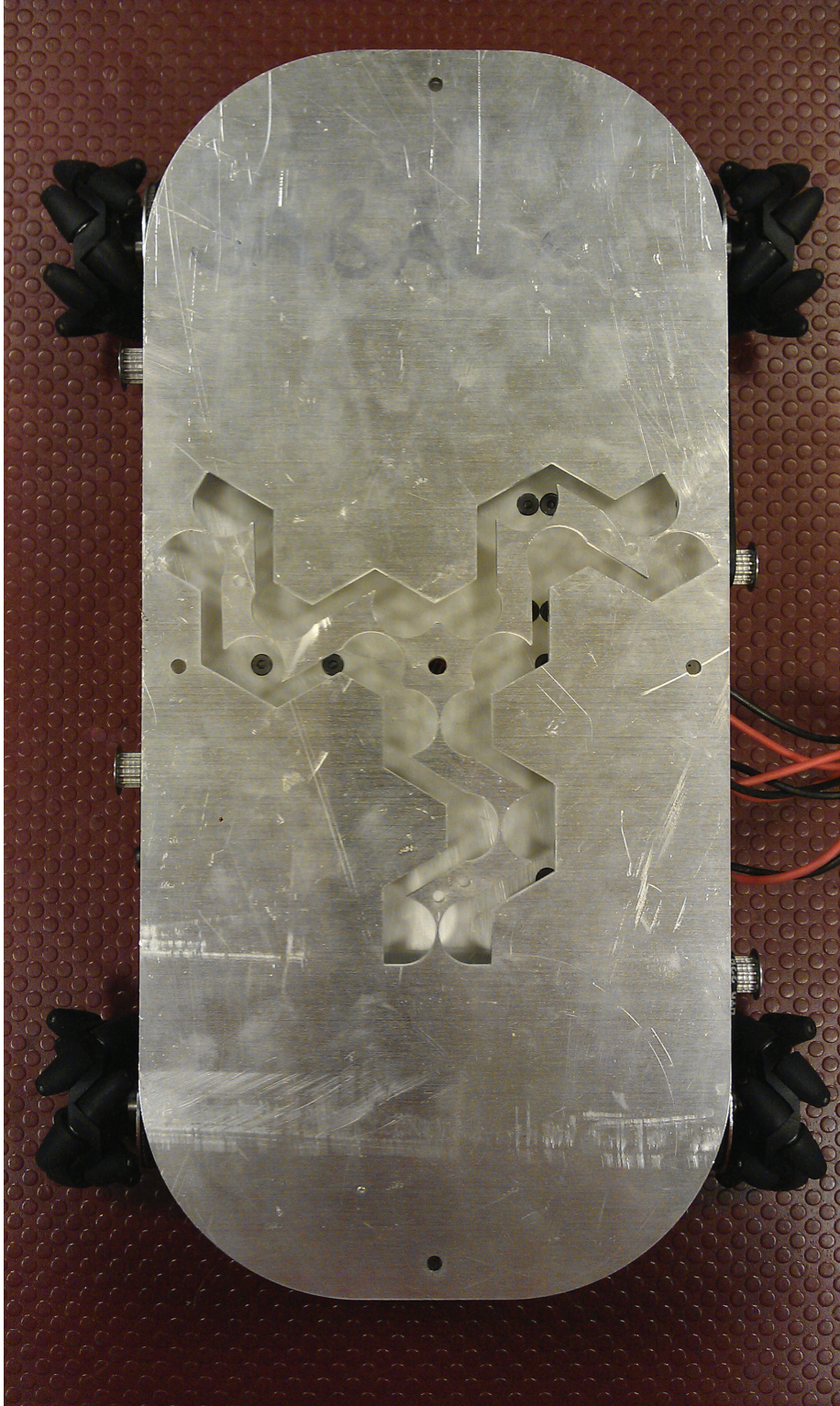


Figure 3.5: Front view of the holonomic mobile platform with series elastic actuation.

The second prototype of the mobile platform, shown in Figures 3.5 and 3.4, is designed to address the shortcomings of the first design. The footprint of the robot is reduced by 43% with respect to the first prototype. Specifically, the robot length is kept constant to locate the whole forearm while the robot width is reduced to 160mm's which is just enough to fit the forearm on top of the robot. In parallel with the robot width, weight of the robot is decreased to 4.2 kg. In order to achieve the reduced footprint area, the actuators are placed asymmetrically, while keeping the wheel configurations symmetric. Moreover, the robot is produced from high quality 7075 series aluminum to increase robustness.

To improve localization performance, two optical flow sensors are placed under the robot. Each sensor is capable of measuring position changes on both  $x$  and  $y$  directions. Using two sensors, the rotation of the platform can also be estimated. The optical flow sensors enable measurement of the task space coordinates of the robot correctly even under wheel slip and increase the accuracy of localization estimation.

Finally, the second prototype utilizes SEA, alleviating the need for a high cost force sensor. To implement SEA, a compliant element based on a compliant mechanism is introduced to the top of the mobile platform and its deflections are measured using linear encoders. The implementation details of the compliant mechanism is explained in Section 3.2.2.

The design of connecting parts that enable human arm attachment are also modified in the second prototype. The new design enables the whole forearm rest on the platform using elastic bandages. In addition the end effector of the robot is moved to the front of the mechanism from the robot center.

### Design of the Compliant Element of SEA

A 3 –  $\underline{RRR}$  planar parallel compliant mechanism, shown in Figure 3.7, is selected as the underlying kinematics of the compliant element. The analytic kinematic solution of the 3 –  $\underline{RRR}$  parallel planar mechanism is derived as in [69]. The compliant mechanism is based on a monolithic design and features notch hinge joints as shown in Figure 3.6. Task space stiffness and maximum joint deflections of the compliant mechanism are derived following [59]. In particular, the maximum deflection of the notch hinge joint is analytically calculated as,

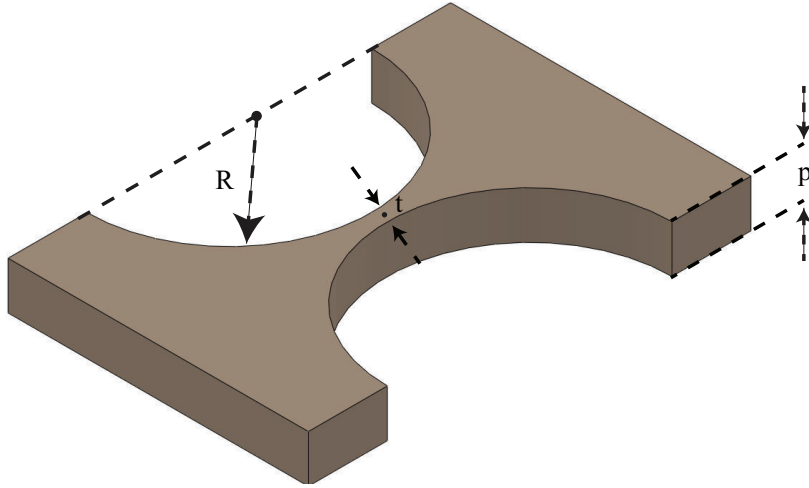


Figure 3.6: CAD model of compliant notch-hinge joint used to implement compliant 3 –  $\underline{RRR}$  mechanism

$$\theta_{max} = \frac{3\pi}{4E} \sqrt{\frac{R}{t}} \sigma_{max} \quad (22)$$

where  $\theta_{max}$  is the maximum deflection angle,  $R$  is the radius of the joint,  $t$  is the hinge width,  $E$  is the Young's modulus and  $\sigma_{max}$  is the maximum stress of the selected material.

The stiffness of each notch-hinge joint reads as,

$$K_{joint} = \frac{2Ep}{9\pi} \sqrt{\frac{t^5}{R}} \quad (23)$$

where  $K_{joint}$  is the joint space stiffness,  $p$  is the depth of the joint.

Finally, the maximum task space stiffness of the compliant mechanism is derived using maximum joint stiffness and motion level kinematic analysis of the 3 –  $\underline{RRR}$  mechanism.

In particular, each joint is designed to have  $2.84^\circ$  maximum deflection angle and  $5.093Nm/rad$  joint stiffness. The joint deflections of the compliant mechanism are measured using linear encoders with 500 counts per inches resolution.

In order to find the task space stiffness of the compliant SEA mechanism, the Jacobian matrix for measured and passive joints should be derived for both active (measured) and passive joints. The Jacobian matrix can be written explicitly as,

$$\begin{bmatrix} \Delta x_T \\ 0 \end{bmatrix} = \begin{bmatrix} J_{T_a} & J_{T_p} \\ J_{C_a} & J_{C_p} \end{bmatrix} \begin{bmatrix} \Delta q_a \\ \Delta q_p \end{bmatrix}$$

where  $J_{T_a}$  is the Jacobian matrix for unconstrained measured joints,  $J_{T_p}$  is the Jacobian matrix of unconstrained passive joints,  $J_{C_a}$  is the Jacobian matrix for constrained measured joints and  $J_{C_p}$  is the Jacobian matrix for constrained passive joints. In 3 –  $\underline{RRR}$  case,  $J_{T_a}$  is a  $3 \times 3$  square matrix with distinct eigenvalues,  $J_{T_p}$  is a  $3 \times 6$  long matrix,  $J_{C_a}$  is a  $6 \times 3$  long matrix and  $J_{C_p}$  is a  $6 \times 6$  square matrix with distinct eigenvalues. Using these matrices

the constrained Jacobian matrix is derived as,

$$\begin{aligned}\Delta x_T &= (J_{T_a} - J_{T_p} J_{C_p}^{-1} J_{C_a}) \Delta q_a \\ &= J_{T_{comp}} \Delta q_a\end{aligned}$$

where  $J_{T_{comp}}$  is the Jacobian matrix of the compliant mechanism. Once the Jacobian matrix of the compliant mechanism is obtained, the task space stiffness of can be derived as

$$K_T = J_{T_{comp}}^{-T} (K_{q_a} + J_{C_a}^T J_{C_p}^{-T} K_{q_p} J_{C_p}^{-1} J_{C_a}) J_{T_{comp}}^{-1} \quad (24)$$

where  $K_T$  is the task space stiffness matrix of the compliant mechanism,  $K_{q_a}$  and  $K_{q_p}$  are the individual stiffness values of measured and passive joints and equal to  $K_{joint}$  since all joints are identical. Using the above equation the task space stiffness values are derived as,  $42N/mm$  along  $x$  and  $y$  directions and  $25Nm/rad$  about the rotational axis.

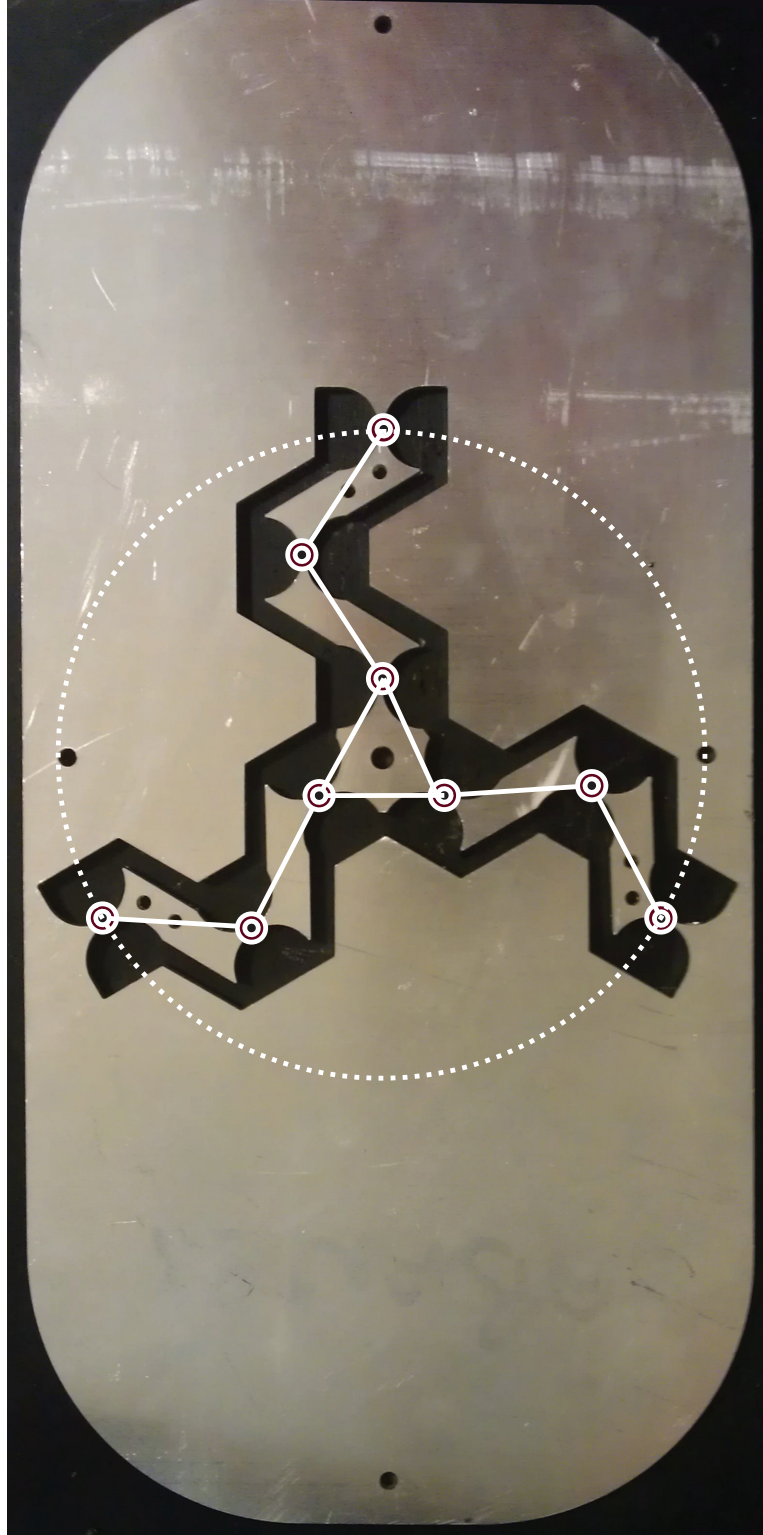


Figure 3.7: Top view of the compliant 3 –  $\underline{RRR}$  mechanism that is used to estimate forces along  $x$  and  $y$  directions and the torque about the perpendicular axis.



Figure 3.8: Final design of the holonomic mobile platform with SEA. Holonomic platform can be easy to attach to patients using elastic bandages.

## Verification of Force Sensing based on Compliant Mechanism

In order to verify the force sensing fidelity of compliant element, a test-bed is prepared such that force estimates of the compliant mechanism can be compared to commercial 6 axis ATI Nano17 force/torque sensor. In particular, the forces/torque applied to the compliant mechanism are estimated using end-effector stiffness and measurements of the deflection of the grounded links of the compliant mechanism. Given the deflections of the grounded links, the end-effector deflections are calculated using the forward kinematics. Figures 3.9, 3.10 and 3.11 present the measurements of the force sensor along with the force estimates through the compliant element along  $x$ ,  $y$  and  $\theta$  directions, respectively. Results indicate that force estimates through the compliant element can track the applied forces quite well as long as the applied forces are below some threshold. When the forces are increased the error in the force estimates increases. Such an error is expected, since the analysis of the compliant mechanism strongly depends on the assumption of small deflections.

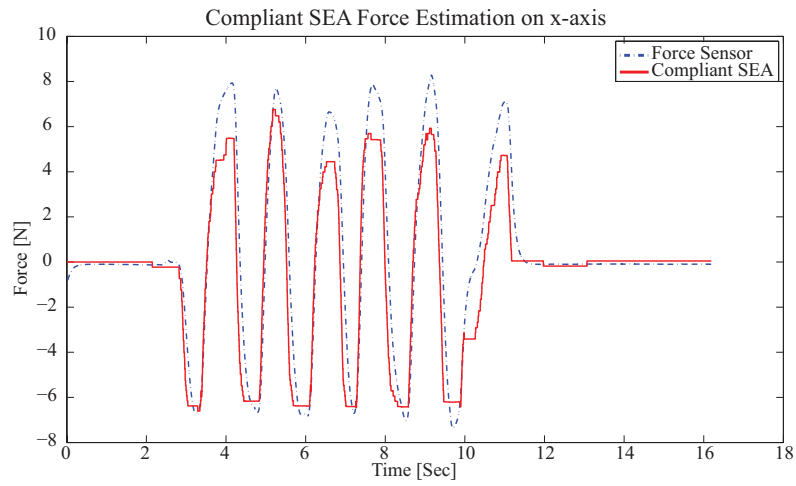


Figure 3.9: Experimental comparison of the applied and estimated forces along the  $x$ -axis.

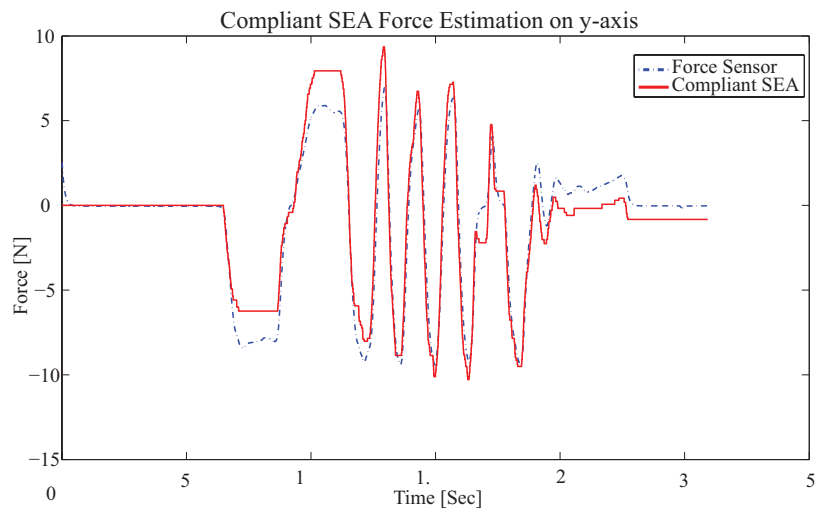


Figure 3.10: Experimental comparison of the applied and estimated forces along the  $y$ -axis.

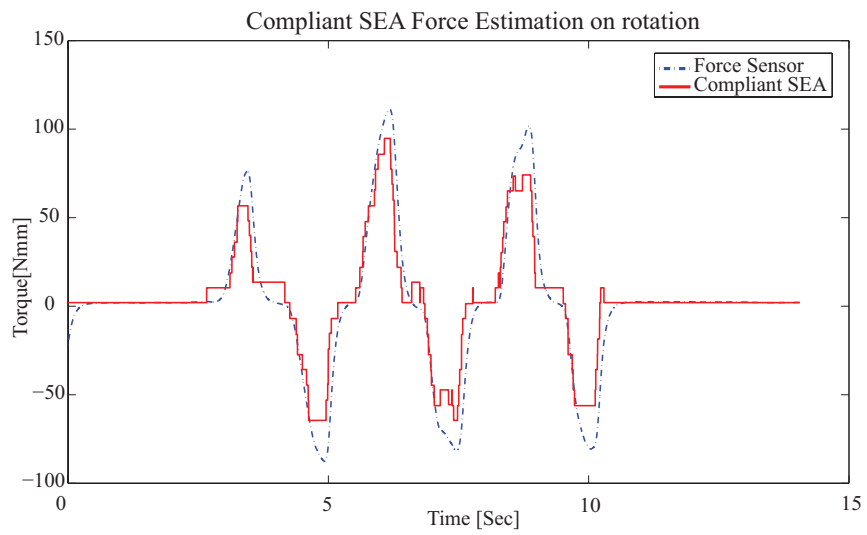


Figure 3.11: Experimental comparison of the applied and estimated torques.

# Chapter IV

## 4 Controller Synthesis, Characterization and VR Integration

This chapter consists of three parts. In Section 4.1 controller synthesis for the knee exoskeleton is presented. The controllers of the holonomic mobile platform are detailed in Section 4.2. Finally, in Section 4.3 the experimental characterization results are reported.

### 4.1 Control of the Knee Exoskeleton

This section presents impedance controller synthesis, verification of force rendering fidelity and usability tests with human subject experiments for the knee exoskeleton.

#### 4.1.1 Impedance Controller

Thanks to the use of back-driveable and low inertia motors and utilization of a low transmission ratio, the robot prototype is highly back-driveable. As a result, it is possible to implement a model-based open-loop impedance controller for the device to control interaction forces, alleviating the need for force sensors. The overall control architecture used to control the device is depicted in Figure 4.1. Note that to increase the fidelity of impedances

rendered by the impedance controller, the end-effector can still be equipped with a force/torque sensor enabling implementation of closed-loop impedance control. However, such an implementation drastically increases the cost.

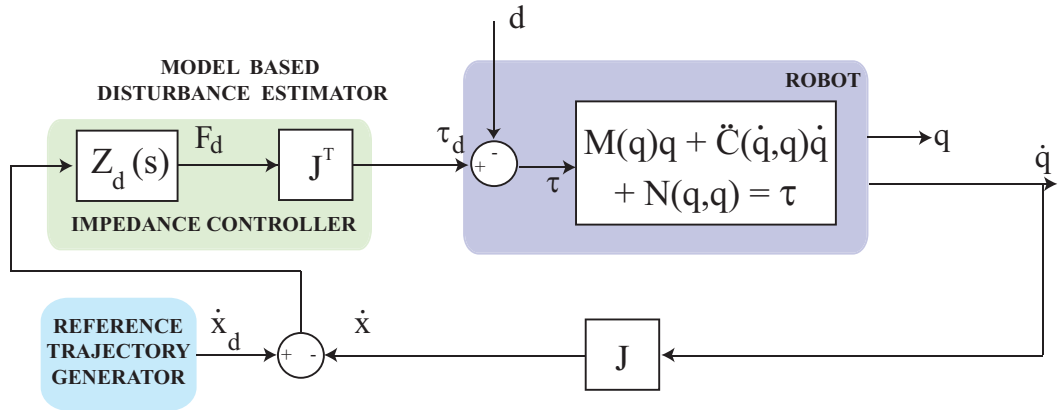


Figure 4.1: Block diagram of the impedance control architecture

In Figure 4.1,  $q$ ,  $\dot{q}$  represent the actual position and velocity of the joints,  $\dot{x}$  and  $\dot{x}_d$  represent the actual and desired task space velocities,  $F_d$  denotes desired forces acting on the robot,  $J$  is the robot Jacobian matrix,  $\tau$  and  $\tau_d$  are the actual and desired actuator torques,  $M$  is the robot mass matrix,  $C$  and  $\hat{C}$  are the actual and modeled centrifugal and Coriolis matrices,  $N$  and  $\hat{N}$  are the actual and modeled gravity forces.  $u_{ff}$  is the feed-forward compensation term from model-based disturbance estimator, while  $d$  represents the physical disturbances acting on the system. In the control architecture, the measured actuator velocities are multiplied with the Jacobian matrix and the actual end-effector velocities are obtained. The difference of the actual and desired end-effector velocities are fed to the impedance controller and desired forces are calculated. Then, desired forces are multiplied with the Jacobian transpose matrix and desired joint torques are obtained. The desired joint torques are added with the feed-forward torques estimated using

the dynamic model of the robot, that is, Coriolis, centrifugal and gravity matrices. Since disturbances acting on the robot are physical and change according to the environment, the total torque applied to the physical robot includes these parasitic effects. If a force sensor is available to measure the forces applied at end-effector, then the difference between the measured and desired values of the forces can be fed to a force controller, implementing a closed-loop controller.

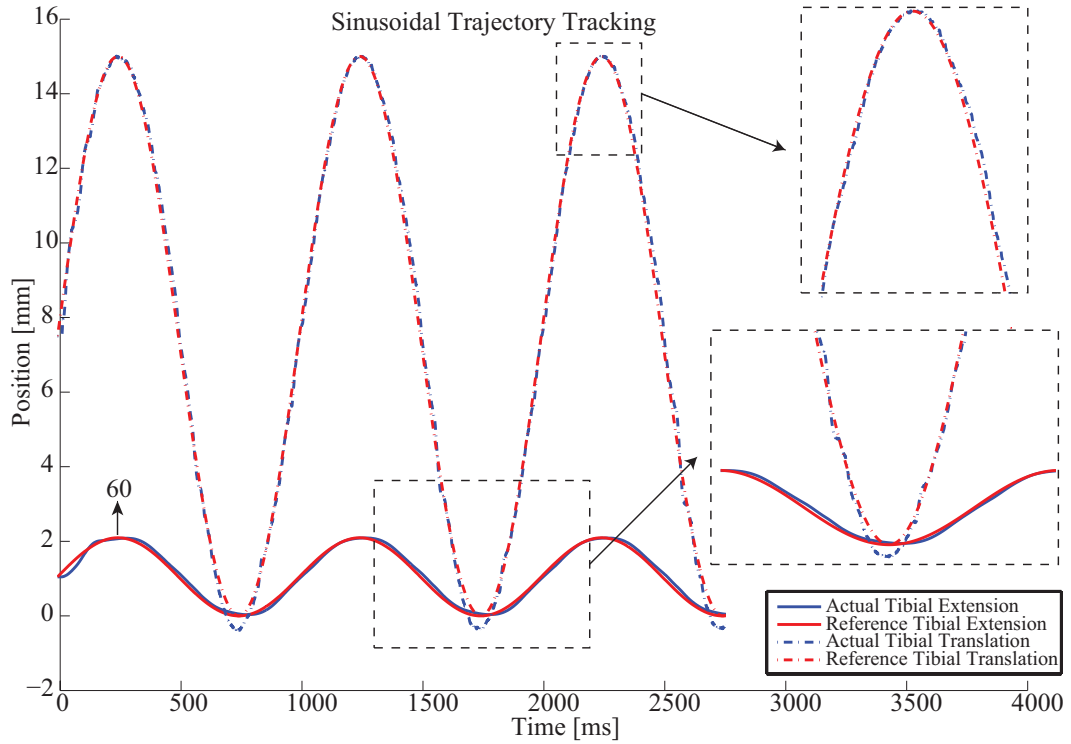


Figure 4.2: The path used to test position tracking performance is a simulation of the tibial translation of the knee joint. In the desired path, the center of knee joint translates up to 15mm during a  $60^\circ$  knee extension at 1Hz.

In order to verify the position tracking performance of the controller, a possible trajectory for the knee joint is modeled. In particular,  $60^\circ$  rotation of

the device is commanded simultaneously with a 15mm translation of the rotation axis. The reference signal is commanded at a frequency of 1 Hz, which ensures sufficiently fast movements for knee rehabilitation. Figure 4.2 depicts the tracking performance of the controllers. For the experiment presented, the RMS values of the tracking error are calculated as 1.8% in translation and 7.5% in rotation.

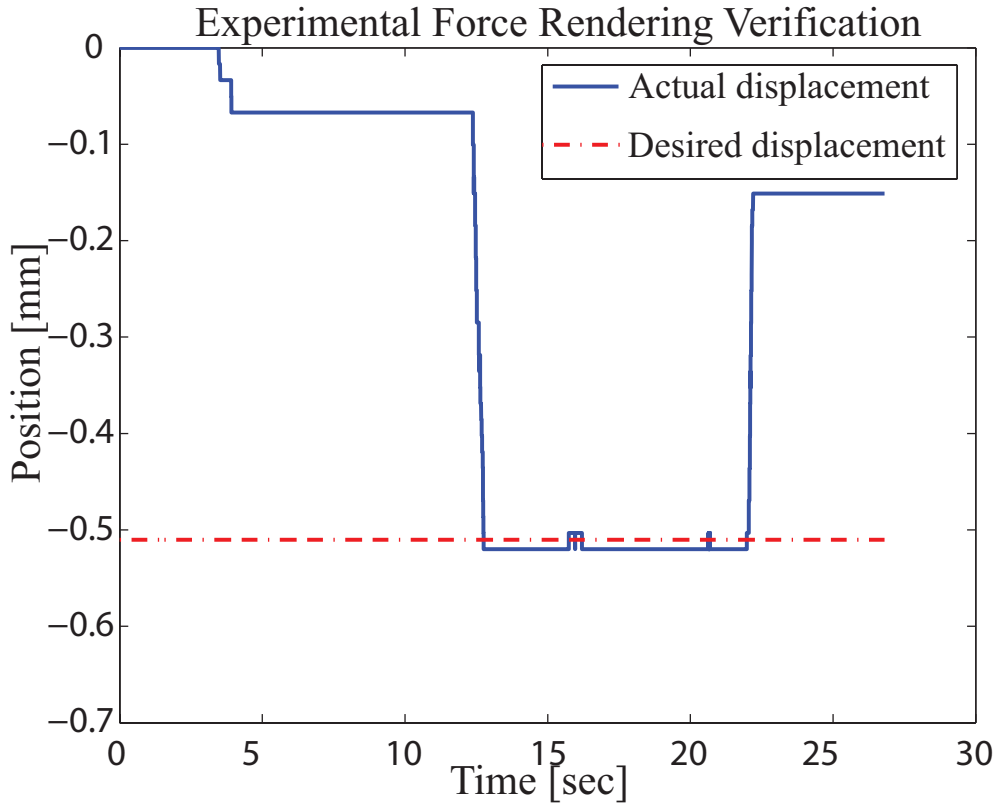


Figure 4.3: The knee exoskeleton is modeled as a spring with 10 kN/m stiffness and a force of 5.1 N is exerted to the end effector of the robot along x-direction. The position change at the end effector is observed as 0.519mm.

In order to verify the force rendering performance of the knee exoskeleton, the robot is modeled as a linear spring with 10000  $N/m$  stiffness along the

$x$  axis. Then, a force of 5.1  $N$  is applied between 13-23 seconds along  $x$  direction. As presented in Figure 4.3, under perfect impedance rendering the end-effector of the exoskeleton is expected to shift 0.510 mm, while The end-effector of the robot has shifted 0.519 mm, indicating a 1.87% error in rendered force. Since the error in the rendered force is small, we can conclude that the knee exoskeleton has a good force rendering performance even under open-loop force control.

#### 4.1.2 Human Subject Experiments

Human subjects experiments are carried out to measure the rotations and translations of the knee joint on the sagittal plane. The knee exoskeleton have been tested with three volunteers. All volunteers are male, with ages between 23-29, and have a height between 175-185 cm. Since the experiments are designed to show the useability and ergonomy of knee exoskeleton, all volunteers are unimpaired with no history of knee problems. Volunteers are attached to the knee exoskeleton using elastic strips. These strips not only ensure an ergonomic attachment but also allow for small passive movements along the axis the perpendicular to sagittal plane. The volunteers completed flexion/extension movements of their knee while sitting. In the trials, the speed of the movements were not imposed, since the coupling between knee joint translations and rotation are independent from the speed of the movement.

Figure 4.4 presents measurements from the first volunteer. Measured knee movements clearly show the translation of rotation axis during flexion/extension movements. Note that the translations and rotation are coupled but no simple correlation exist between these motions of the knee.

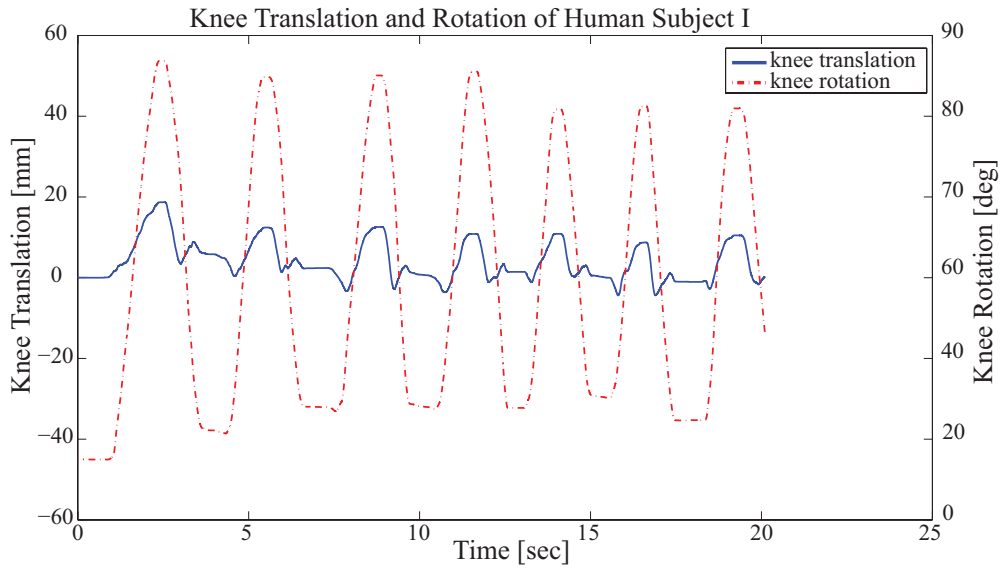


Figure 4.4: Coupled translations and rotation of the knee of the first volunteer.

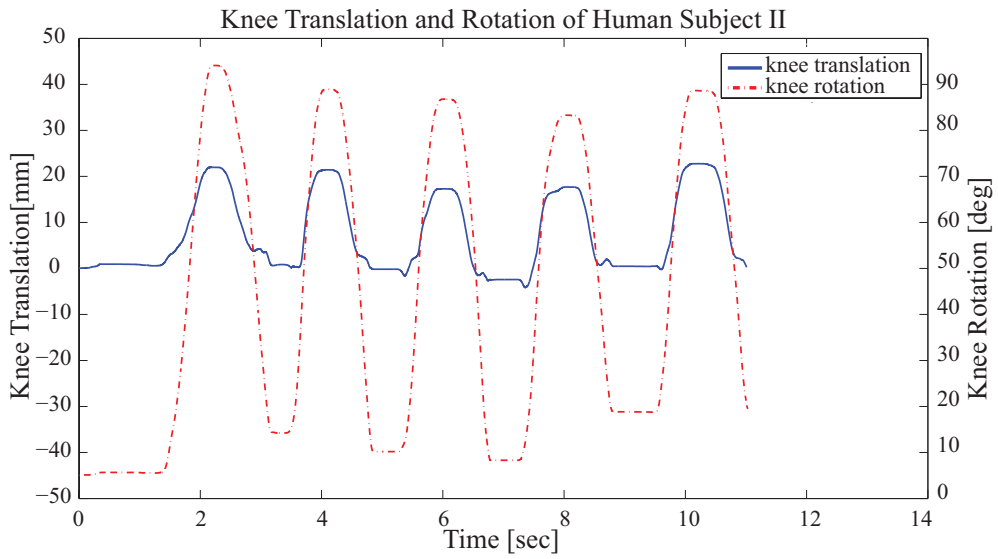


Figure 4.5: Coupled translations and rotation of the knee of the second volunteer.

Figure 4.5 presents measurements from the second volunteer. Once again translation of rotation axis during flexion/extension movements can be observed from these measurements. However, the coupling between translations and rotations have a much different characteristic than the coupling for the first subject. Moreover, the magnitude of translations are also different. Such differences are expected since the coupled motion of the knee depend on the shape of articulated surfaces and ligament structure of the knee, and is unique to each individual.

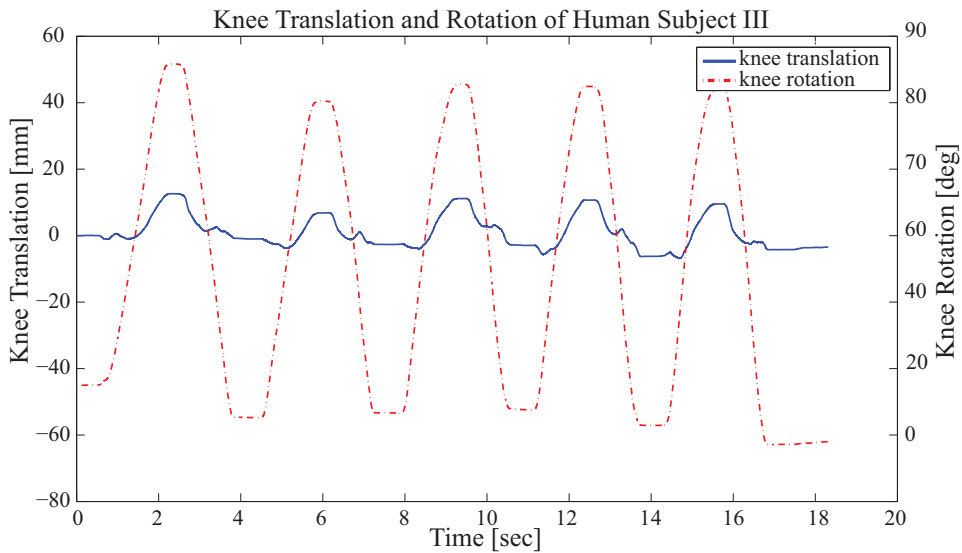


Figure 4.6: Coupled translations and rotation of the knee of the third volunteer.

Figure 4.6 shows knee translation/rotation movements for the third volunteer. As expected, the coupled knee movements of this volunteer are also different from the other volunteers in both magnitude and translational path.

## 4.2 Control of the Mobile Platform

This section details the controllers synthesized for holonomic mobile platform. In particular, admittance control, series elastic actuation, passive velocity field control and virtual tunnels are covered.

### 4.2.1 Admittance Control

To ensure back-driveability of the robot under the action of human interaction forces at the robot end-effector, an admittance controller is synthesized and implemented. Figure 4.7 presents the block diagram of the this controller. In the figure,  $M$  denotes robot inertia matrix, while  $C$  is the Coriolis matrix.  $J$  denotes the Jacobian matrix and  $F_{int}$  is physical interaction force acting on the robot.  $q$ ,  $\dot{q}$ ,  $\dot{q}_c$  and  $\ddot{q}$  represent the actual position and velocity, compensated velocity and actual acceleration of the DC motors, while  $\dot{x}$ ,  $\dot{x}_d$  and  $\dot{x}_c$  denote actual, desired and compensated task space velocities of the robot.  $\xi_q$  and  $\xi_f$  signify the noise acting on position  $q$  and force  $F_s$  measurements.  $K_d$  is the desired impedance of the system,  $C_{com}$  is the admittance compensator, while  $D$  denotes the velocity controller block.  $u$  represents the torques calculated by velocity controller and  $\tau$  denotes net the torques acting on the robot. Finally  $d$  is the disturbance acting on the system.

The admittance controller in Figure 4.7 inputs the desired velocities in task space and feeds the error in the task space velocity to the desired impedance of the robot. The resulting force is compared with the force sensor measurements and the force error is fed to the pre-determined admittance of the robot. The velocity level controller first combines the reference velocity with the velocity of the admittance and determines the compensated joint velocities. Then, compensated joint velocities are compared with actual

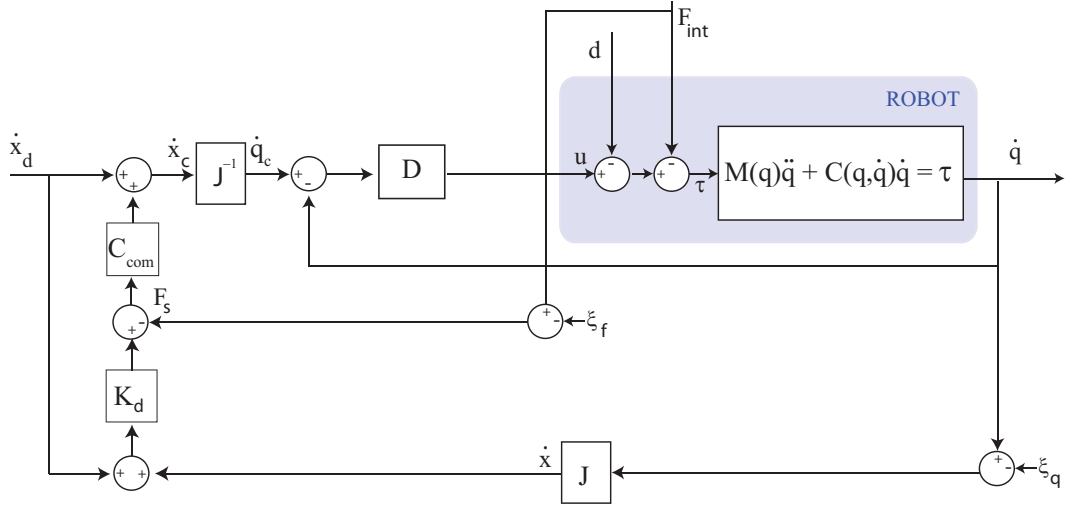


Figure 4.7: Block diagram of the admittance controller

joint velocities and the error is regulated by a PI controller.

The admittance controller is implemented on both prototypes of the holonomic platform. The controller allows the robot to operate in assistive and resistive modes by simply changing the parameters of the admittance compensator. To test the admittance controller, a virtual tunnel is implemented by introducing virtual constraints at  $\pm 50mm$  from the  $x$ -axis, that is, defining forbidden regions in the task space of the mobile platform. The virtual tunnel is a straight corridor with  $100mm$  width and  $800mm$  height. Figure 4.13 presents experimental results, where the path followed by the robot is depicted along with the forces applied by the patient.

It can be observed from Figure 4.13 that the movement of the mobile platform follows the interaction forces applied at the end-effector. Moreover, whenever the patient reaches the boundary of the virtual tunnel, the controller pushes the robot inside the tunnel, successfully implementing virtual fixtures. Finally, the robot is highly back-driveable within the bandwidths of

human user and can be easily directed with the application of small forces.

#### 4.2.2 Series Elastic Actuation

In the literature, series elastic actuators have been controlled using various control methods, ranging from PID control to impedance control techniques. In [51], Pratt implemented a standard PID controller with feed-forward terms that are introduced to compensate for the nonlinearities of the input signal. In [70], Sensinger et. al. utilized impedance control for a SEA whose intrinsic impedance is low. Similarly in [71], Pratt et. al. used an impedance controller for a SEA and showed that voltage drive mode results in better performance than torque drive mode. In [72], Wyeth showed that a position loop can be placed inside the force control loop so that the motor can be treated as a pure velocity source and the design of the outer control loop can be simplified. In [73], Vallery et. al. used the control structure proposed by Wyeth, and proposed conditions to ensure the passivity of the SEA. In particular, a PI controller is used for the inner velocity loop while the outer loop is synthesized utilizing the passivity analysis.

The SEA controller used for the holonomic mobile platform is synthesized shown in Figure 4.8. In the cascaded structure of Figure 4.8, there is an inner

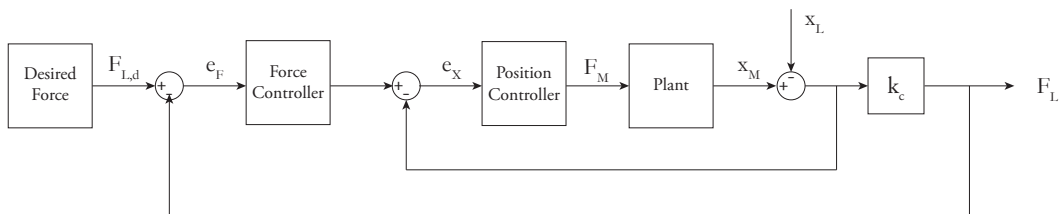


Figure 4.8: Block diagram of the SEA controller

position control loop and an outer force control loop. The inner loop of the

control structure deals with imperfections (friction, stiction, etc). In other words, inner control loop turns system into an effective position source, [72]. On top of this control loop, a force controller is implemented.

### 4.2.3 Passive Velocity Field Controller

There exists several control techniques for path following tasks. Among the available approaches, passive velocity field control (PVFC) is of particular interest, since this method not only minimizes the contour error but also does so by rendering the close loop system passive with respect to externally applied forces. PVFC concept has been first proposed as a part of a smart exercise protocol in [74] and further analyzed in [75,76]. Later, PVFC has been adapted to bilateral control [77,78]. In [79], the controller has been further extended to include shaping of the *potential energy* of the closed loop system dynamics as well as its kinetic energy. Finally, in [80], a PVFC controller that operates solely on joint positions has been proposed, alleviating the need for velocity measurements. The PVFC controller used in the holonomic mobile platform is an implementation of the controller proposed in [81,82].

In PVFC, the task to be performed and speed of the task are decoupled from each other. In particular, the task is embedded in a predefined velocity field while the speed depends on the instantaneous energy of the closed loop system. For example, for human-in-the-loop contour following tasks, a predefined velocity field encodes the path to be followed, while the initial energy of the system and the work done by the human operator on the system dictates the speed of motion. PVFC mimics the dynamics of a flywheel; hence cannot generate energy, but can store and release energy supplied to it. As a consequence, the controller renders the close-loop system passive

*with respect to externally applied forces.* This is one of the unique features of PVFC approach, as classical passivity-based robot control laws [83–85] cannot guarantee passivity when external forces are considered as the input. Passivity with respect to external forces is crucial in human-machine interaction, since it enhances safety by limiting the amount of energy that can be released to the operator, especially in case of an unexpected system failure.

Given the dynamics of the manipulator as

$$M(q)\ddot{q} + C(q, \dot{q})\dot{q} = \tau + \tau_e \quad (25)$$

where  $M(q) \in \mathbb{R}^{n \times n}$  is the inertia matrix,  $C(q, \dot{q}) \in \mathbb{R}^{n \times n}$  is the Coriolis matrix,  $\tau$  represents control forces, and potential forces are embedded in the external force  $\tau_e$ , PVFC renders the controlled manipulator as a dynamic non-linear impedance that can store and release the energy supplied to it. Thanks to this property, the control law guarantees passivity with respect to the supply rate  $s(\tau_e, \dot{q}) = \tau_e^T \dot{q}$ , that is, it ensures passivity with respect to external force inputs  $\tau_e$ , implying

$$\int_0^t \tau_e^T \dot{q} d\tau \geq -c^2 \quad (26)$$

where  $c$  is some real number.

In PVFC, the desired task and the speed of task execution are decoupled. For instance, for a contour following task, the desired path is encoded into the velocity field, so that for each location of the robot end-effector, a proper reference trajectory can be calculated, while the controller ensures that the velocity of the robotic manipulator converges to a scaled multiple of this desired velocity in the absence of external forces: Formally, the controller

guarantees that for any initial condition  $(q(0), \dot{q}(0))$ , there exists a constant  $\rho > 0$  s.t.

$$\lim_{t \rightarrow \infty} \dot{q}(t) - \rho V(q(t)) = 0. \quad (27)$$

when  $\tau_e \equiv 0$ . Note that the parameter  $\rho$  dictates the speed of task execution and can be positive or negative. The magnitude of  $\rho$  is governed by the instantaneous energy of the system; hence, can be adjusted either by changing the initial conditions of the system or through external forces doing (possibly negative) work on the system. This implies, for contour following tasks, the desired path can be traced forwards and backwards by simply changing the sign of the gain, and at different speeds by tuning the instantaneous energy of the system through controlled variables.

### Coupling Control Law

Given an augmented velocity field, the skew-symmetric control law is calculated using two terms; the role of the first term  $\bar{\tau}_c$  is analogous to feed-forward dynamic compensation while the second term  $\bar{\tau}_f$  forces the error dynamics to converge. In particular,

$$\bar{\tau}(\bar{q}, \dot{\bar{q}}) = \bar{\tau}_c(\bar{q}, \dot{\bar{q}}) + \bar{\tau}_f(\bar{q}, \dot{\bar{q}}) \quad (28)$$

with

$$\bar{\tau}_c = \frac{1}{2\bar{E}} \underbrace{(\bar{w}\bar{P}^T - \bar{P}\bar{w}^T)}_{\text{skew symmetric}} \dot{\bar{q}} \quad (29)$$

$$\bar{\tau}_f = \gamma \underbrace{(\bar{P}\bar{p}^T - \bar{p}\bar{P}^T)}_{\text{skew symmetric}} \dot{\bar{q}} \quad (30)$$

where  $\gamma \in \mathbb{R}$  in Eqn. (30) is a control gain, not necessarily positive, which determines the convergence rate and the sense in which the desired velocity field will be followed.

In Eqns. (29) and (30),  $\bar{p}$  denotes the momentum of the augmented system, while  $\bar{P}$  is the desired momentum of the augmented system. The symbol  $\bar{w}$  represents the inverse dynamics necessary to follow the desired velocity field. Mathematically,

$$\bar{p}(\bar{q}, \dot{\bar{q}}) = \bar{M}(\bar{q})\dot{\bar{q}} \quad (31)$$

$$\bar{P}(\bar{q}) = \bar{M}(\bar{q})\bar{V}(\bar{q}) \quad (32)$$

$$\bar{w}(\bar{q}, \dot{\bar{q}}) = \bar{M}(\bar{q})\dot{\bar{V}}(\bar{q}) + \bar{C}(\bar{q}, \dot{\bar{q}})\bar{V}(\bar{q}) \quad (33)$$

where the  $i^{th}$  component of  $\dot{\bar{V}}$  is calculated as

$$\dot{\bar{V}}_i(\bar{q}) = \sum_{k=1}^{n+1} \frac{\partial \bar{V}_i(\bar{q})}{\partial \bar{q}_k} \dot{\bar{q}}_k. \quad (34)$$

In [75], it has been proven that the skew symmetric control law coupled with the skew symmetry property of the robotic manipulators renders the closed-loop system passive with respect to external force inputs and regulates the error dynamics to zero (exponentially) in the absence of external forces. Moreover, it has been shown that the total energy in the system remains constant (as long as no work is done on the system by external forces) and the rate at which the parameterized trajectory progresses is determined by the instantaneous energy of the system. The reader is referred to [75, 76, 86] for stability proofs, robustness analysis and detailed convergence characteristics of PVFC. Convergence of the controller to time varying velocity fields is

further discussed in [79].

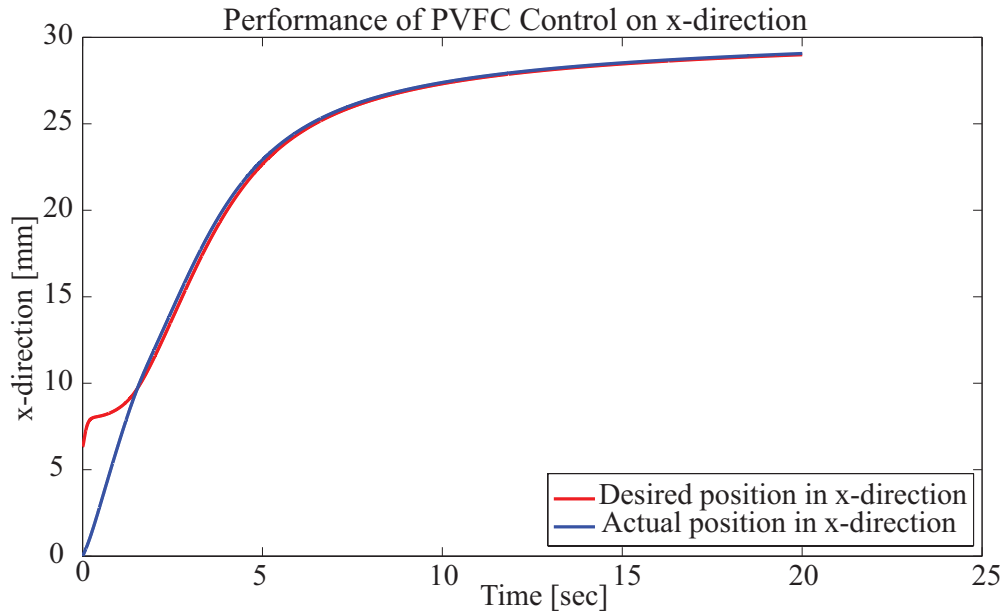


Figure 4.9: Path tracking performance of the holonomic mobile platform in  $x$ -direction under task-space passive velocity field control.

### Simulation Results for Task-space Passive Velocity Field Control of Holonomic Mobile Platform

Path tracking performance of the PVFC of the holonomic mobile platform is tested in simulation. In particular, a PVFC is employed to track curved path as depicted in Figure 4.11. Figure 4.9 and Figure 4.10 present, the path tracking performance of the holonomic mobile platform in  $x$  and  $y$ -directions, respectively. The reference path and the actual robot path on the  $x - y$  plane is also given in Figure 4.11. From the figures, one can observe that the robot converges to the reference path slowly and naturally, unlike a typical trajectory tracking controller.

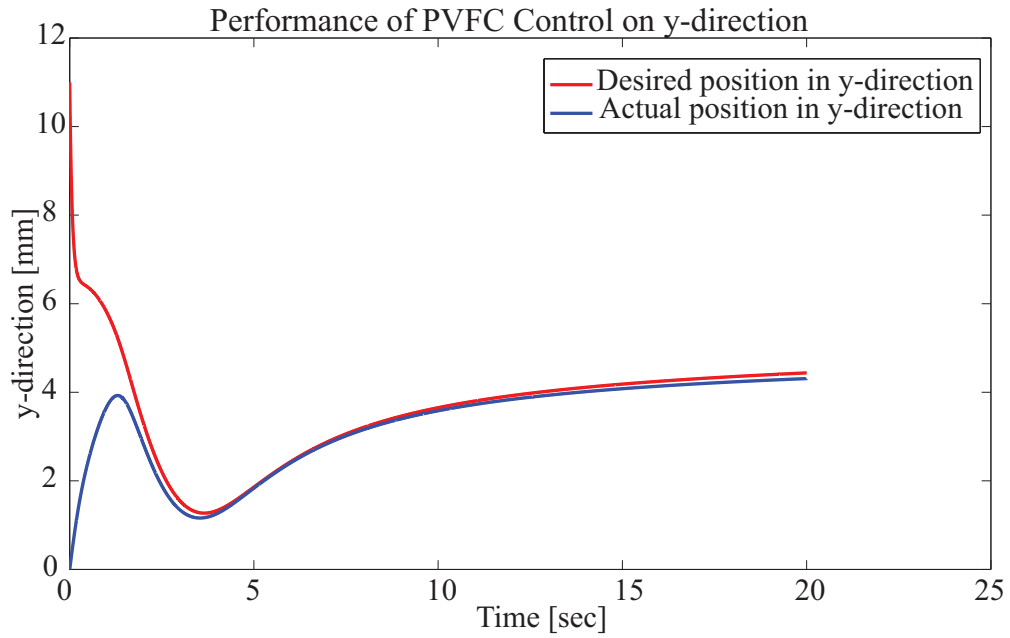


Figure 4.10: Path tracking performance of the holonomic mobile platform in  $y$ -direction under task-space passive velocity field control.

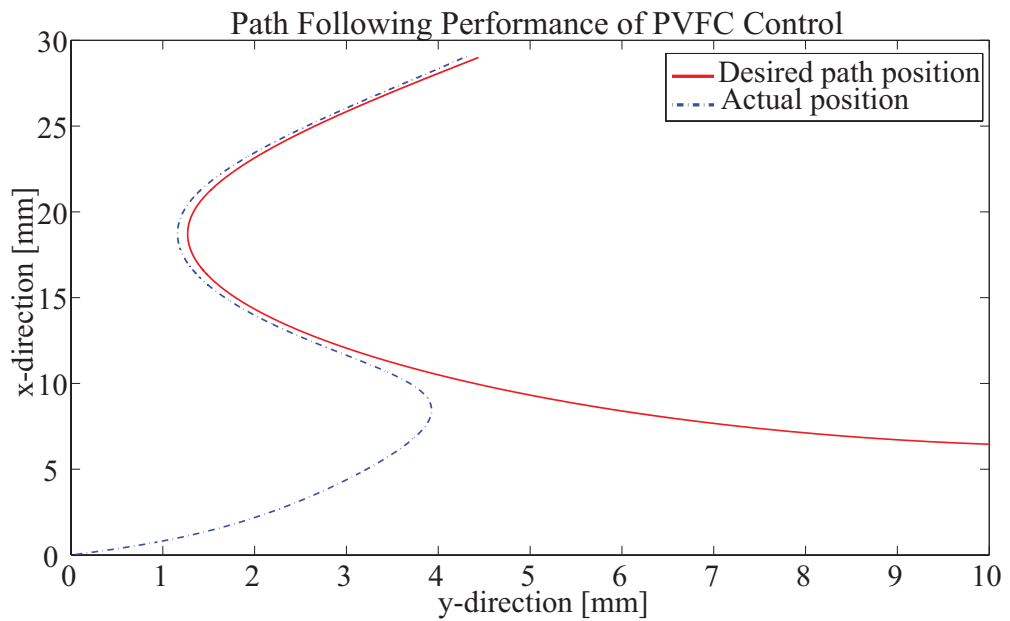


Figure 4.11: Path tracking performance of the holonomic mobile platform on  $x$ - $y$  plane under task-space passive velocity field control.

#### 4.2.4 Virtual Reality Integration of the Mobile Platform

Virtual tasks are modeled in VRML2.0 and controllers are integrated with virtual simulations to support force-feedback rehabilitation therapies. Figure 4.12 presents a screen shot of a sample virtual reality game of a hold, rotate, place and drop scenario, coupled to the holonomic platform. The game features virtual tunnels and force fields within the virtual tunnels. Moreover, feedback about the success of the actions, as well as the quality of the performance are presented to the patient, to encourage participation and to promote concentration.

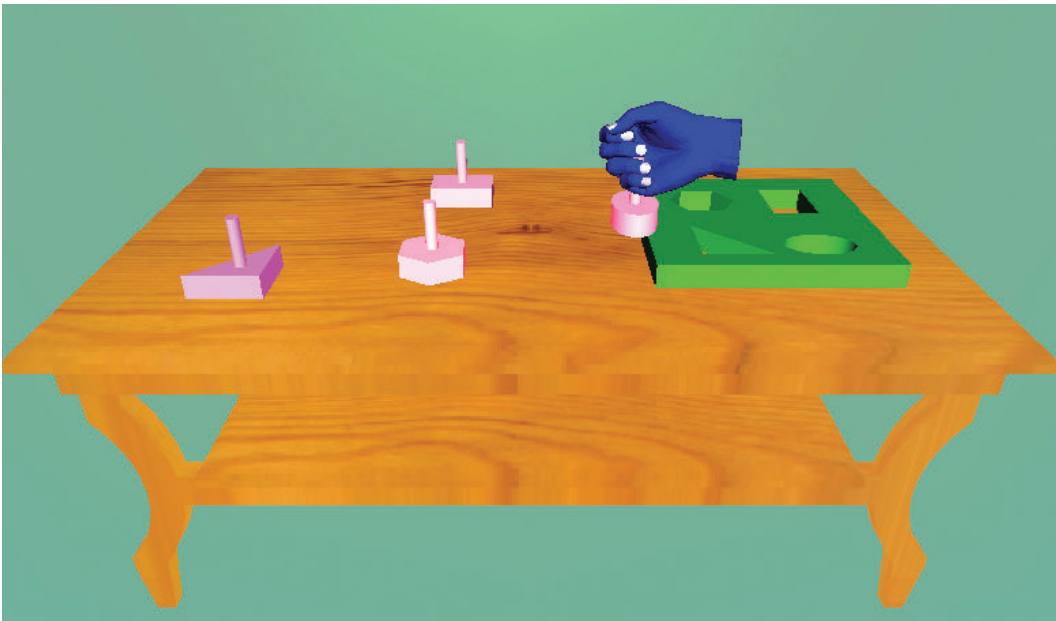


Figure 4.12: Screen shot of a hold, rotate, place and drop game

### 4.3 Experimental Characterization

In this section, experimental characterization results of the knee exoskeleton and the holonomic mobile platform are presented.

#### 4.3.1 Experimental Characterization of the Knee Exoskeleton

Table 4.1: Characterization Table for the 3-RRP Knee Exoskeleton

Criteria	X	Y	Z
Inst. Peak Force	246.7 [N]	213.5 [N]	38.2 [Nm]
Max. Cont. Force	18.4 [N]	16 [N]	2.85 [Nm]
End-Eff. Resol.	0.058 [mm]	0.100 [mm]	0.0031 [rad]
Reach. Worksp.	-60 to 60 [mm]	-60 to 60 [mm]	$\infty$ [rad]
Virt. Wall Rend.	50 [kN/m]	42 [kN/m]	1 [kNm/rad]
Back-driveability	3 [N]	3 [N]	0.25 [Nm]

Table 4.1 presents the experimental characterization results of the 3-RRP knee robot. Instantaneous peak and continuous end-effector forces along  $x$  and  $y$  directions are determined as 246.7 N and 18.4 N, respectively. Similarly, instantaneous peak and continuous end-effector forces along the rotational axis are found as 38.2 Nm and 2.85Nm, respectively. These force values have also been experimentally verified at critical points of the prescribed workspace. The end-effector resolutions are calculated to be 0.3252 mm along  $x$ , 0.5633 mm along  $y$  directions and 0.0031 rad on the rotational direction. The workspace of the robot spans a range from  $-60$  mm to  $60$  mm along  $x$  and  $y$  directions, while the robot is capable of performing infinite rotations about the perpendicular axis. The stability limits due to the digital

implementation of the virtual wall rendering without damping are observed as 50 kN/m along  $x$  direction, 42 kN/m along  $y$  direction and 1000 kN/rad on the rotational axis. Finally the characterization results verify that robot is highly back-driveable and it can be moved with a 3 N force along  $x$  and  $y$  directions. As a result of being back-driveable, the exoskeleton can ensure safety even under power loss.

### 4.3.2 Experimental Characterization of the Mobile Platform

Table 4.2: Characterization Table for the Holonomic Mobile Platform with Multi-Axis Force/Torque Sensor

Criteria	X	Y	Z
Inst. Peak Force	1.246 [kN]	1.246 [kN]	25.46 [Nm]
Max. Cont. Force	93 [N]	93 [N]	1.9 [Nm]
End-Eff. Resol.	$7 \times 10^{-4}$ [mm]	$7 \times 10^{-4}$ [mm]	$1.7 \times 10^{-4}$ [deg]
Reach. Worksp.	$\infty$ [mm]	$\infty$ [mm]	$\infty$ [deg]
Max. Vel.	1 [m/s]	1 [m/s]	258 [deg/s]
Robot Mass	5 kg		

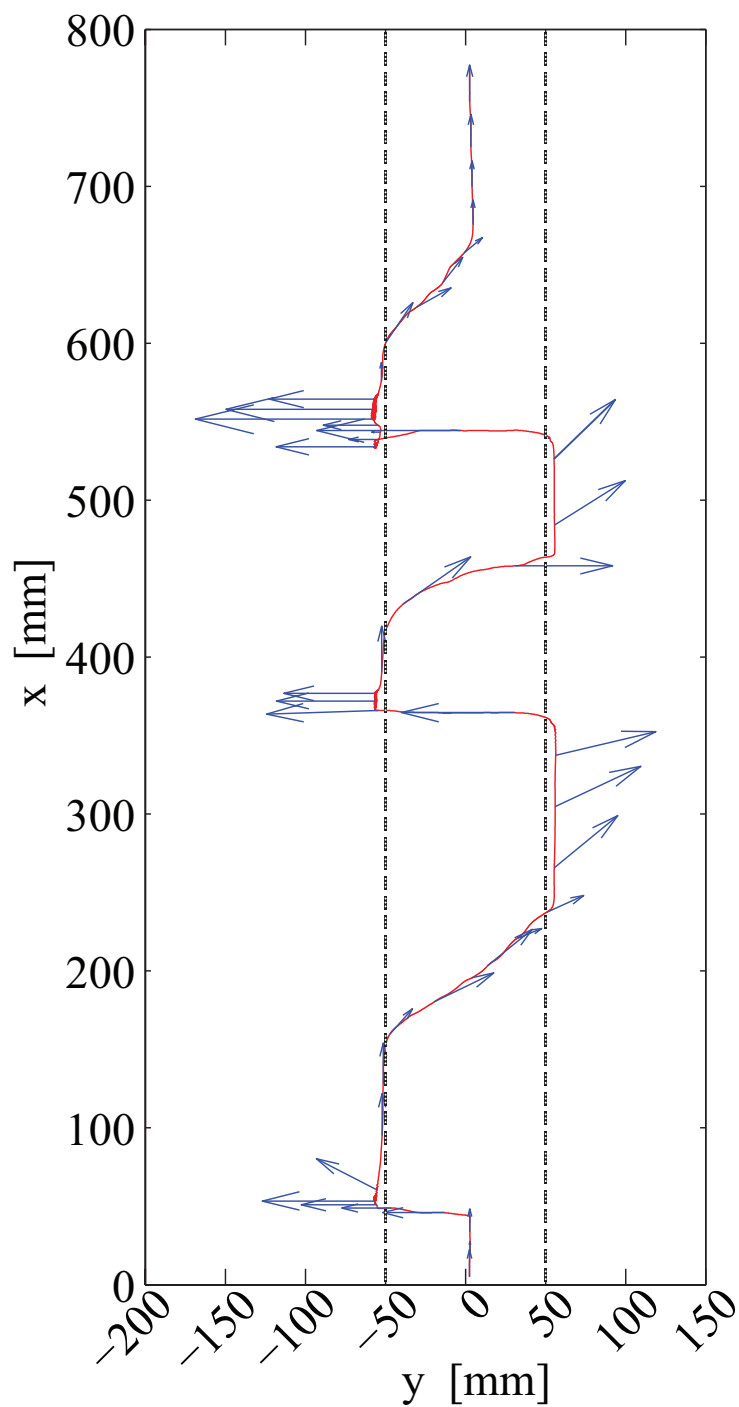
Tables 4.2 and 4.3 list the experimental characterization results of the two different prototypes of the holonomic mobile platform. For the design utilizing multi-axis force/torque sensor, instantaneous peak and continuous end-effector forces along  $x$  and  $y$  directions are determined as 1.246 kN and 93 N, respectively. Similarly, instantaneous peak and continuous end-effector forces along the rotational axis are found as 25.46 Nm and 1.9Nm, respectively. Note that peak forces during physical use are likely to be limited by the wheel slip. The end-effector resolutions are calculated to be  $7 \times 10^{-4}$

mm along  $x$  and  $y$  directions and  $1.7 \times 10^{-4}$  deg on the rotational direction, thanks to 15 bits resolution optical encoders. However, once again the wheel slip will limit the localization performance. The workspace of the robot is infinite since the robot is mobile. The task space velocity of the robot is experimentally verified as 1000 mm/s along  $x$  and  $y$  directions and 4.5 rad/s about its axis of rotation. The mass of the robot is measured as 5 kg. For the

Table 4.3: Characterization Table for the Holonomic Platform with Series Elastic Actuation

Criteria	X	Y	Z
Inst. Peak Force	1.246 [kN]	1.246 [kN]	33.50 [Nm]
Max. Cont. Force	93 [N]	93 [N]	2.5 [Nm]
End-Eff. Resol.	$7 \times 10^{-4}$ [mm]	$7 \times 10^{-4}$ [mm]	$1.7 \times 10^{-4}$ [deg]
Reach. Worksp.	$\infty$ [mm]	$\infty$ [mm]	$\infty$ [rad]
Max. Vel.	1.1 [m/s]	1.1 [mm/s]	4.6 [rad/s]
Robot Mass	4.2 kg		

holonomic mobile platform with series elastic actuation, the instantaneous peak and maximum continuous forces along  $x$  and  $y$  axis and end-effector resolutions do not differ from the first prototype, since the wheel radius and transmission ratio are kept constant. On the other hand, the torques that can be applied at the end-effector are increased due to the change in the robot dimensions. The speed of holonomic mobile platform with series elastic actuation is experimentally determined to be 1100 mm/s along  $x$  and  $y$  directions and 4.6 rad/s about the axis of rotation. The mass of the robot is measured as 4.2 kg.



84  
 Figure 4.13: Path followed by the holonomic mobile platform and the interaction forces applied throughout the motion.

# Chapter V

## 5 Conclusions and Future Work

In this section we review the design of both rehabilitation robots and discuss future works.

### 5.1 The Knee Exoskeleton

We have introduced a novel knee exoskeleton for robot-assisted rehabilitation that accommodates transitional movements of the knee joint along with its rotation. We have shown the effectiveness and applicability of the device by building its prototype and testing its performance under open-loop impedance control. We have also experimental characterized the limits of performance for the device. The results indicate that 3-RRP planar parallel robot is adjustable as claimed and is a good candidate to assist performing knee rehabilitation exercises.

Since the current prototype is implemented only as a proof of concept, the mechanism dimensions are not optimized to minimize the footprint of the robot or to achieve optimal performance. The design of the robot permits volume and footprint reductions at a cost of smaller workspace area. As a part of the future work, the optimal dimensional synthesis of the robot will be performed to comply with the range of motion of the human knee joint and the footprint of the mechanism will be significantly decreased. In the

second prototype of the exoskeleton, disks with thinner profiles will be employed with lower inert timing belts and higher continuous torques will be sustained through use of higher transmission ratios without significantly degrading back-driveability of the device. In addition to the design improvements, extensive human experiments with health volunteers will be conducted to test usability and characterize ergonomics of the device.

## 5.2 Holonomic Mobile Platform

We have developed a 3-DoF, end-effector type, portable, holonomic mobile haptic interface to deliver home based rehabilitation therapies and to administer range of motion/strength exercises for the upper extremity. The device can also be employed to measure patient performance. We have implemented a prototype of the mechanism with series elastic actuation and integrated with virtual reality simulations and can provide assistive/resistive forces to the patient through virtual tunnels designed around nominal task trajectories. We have also synthesized passive velocity field controllers to ensure inherently safe, coordinated and synchronized reaching exercises. Feasibility tests and initial usability studies have been conducted and the efficacy of the device on assisting movements of the arm has been shown. Experience with the device indicates that the device is ergonomic and easy to use.

Future works include studies with stroke patients to test the therapeutic efficacy of the device.

## References

- [1] Global burden of stroke. [http://www.who.int/cardiovascular\\_diseases/en/cvd\\_atlas\\_15\\_burden\\_stroke.pdf](http://www.who.int/cardiovascular_diseases/en/cvd_atlas_15_burden_stroke.pdf).
- [2] Economic cost of stroke. [http://www.who.int/cardiovascular\\_diseases/en/cvd\\_atlas\\_17\\_economics.pdf](http://www.who.int/cardiovascular_diseases/en/cvd_atlas_17_economics.pdf).
- [3] A. Schiele and F.C.T. van der Helm. Kinematic design to improve ergonomics in human machine interaction. *Neural Systems and Rehabilitation Engineering, IEEE Transactions on*, 14(4):456–469, 2006.
- [4] A.H.A. Stienen, E.E.G. Hekman, F.C.T. van der Helm, and H. van der Kooij. Self-aligning exoskeleton axes through decoupling of joint rotations and translations. *Robotics, IEEE Transactions on*, 25(3):628–633, 2009.
- [5] Cathrin Bütefisch, Horst Hummelsheim, Petra Denzler, and Karl-Heinz Mauritz. Repetitive training of isolated movements improves the outcome of motor rehabilitation of the centrally paretic hand. *Journal of the Neurological Sciences*, 130(1):59–68, 1995.
- [6] Gert Kwakkel, Robert C Wagenaar, Jos WR Twisk, Gustaaf J Lankhorst, and Johan C Koetsier. Intensity of leg and arm training after primary middle-cerebral-artery stroke: a randomised trial. *The Lancet*, 354(9174):191–196, 1999.
- [7] A Sunderland, D J Tinson, E L Bradley, D Fletcher, R Langton Hewer, and D T Wade. Enhanced physical therapy improves recovery of arm

- function after stroke. a randomised controlled trial. *Journal of Neurology, Neurosurgery and Psychiatry*, 55(7):530–535, 1992.
- [8] Nestor A. Bayona, Jamie Bitensky, Katherine Salter, and Robert Teasell. The role of task-specific training in rehabilitation therapies. *Topics in Stroke Rehabilitation*, 12(3):58–65, June 2005.
- [9] Johanna H van der Lee, Ingrid AK Snels, Heleen Beckerman, Gustaaf J Lankhorst, Robert C Wagenaar, and Lex M Bouter. Exercise therapy for arm function in stroke patients: a systematic review of randomized controlled trials. *Clinical Rehabilitation*, 15(1):20–31, 2001.
- [10] T. Platz. Evidence-based arm rehabilitation—a systematic review of the literature. *Nervenarzt*, 74(10):841–9, oct 2003.
- [11] G. B. Prange, M. J. Jannink, C. G. Groothuis-Oudshoorn, H. J. Hermens, and M. J. Ijzerman. Systematic review of the effect of robot-aided therapy on recovery of the hemiparetic arm after stroke. *Journal of rehabilitation research and development*, 43(2):171–184, April 2006.
- [12] Gert Kwakkel, Boudewijn J. Kollen, and Hermano I. Krebs. Effects of robot-assisted therapy on upper limb recovery after stroke: A systematic review. *Neurorehabilitation and Neural Repair*, 22(2):111–121, March/April 2008.
- [13] A. Frisoli, F. Rocchi, S. Marcheschi, A. Dettori, F. Salsedo, and M. Bergamasco. A new force-feedback arm exoskeleton for haptic interaction in virtual environments. In *Eurohaptics Conference, 2005 and Symposium on Haptic Interfaces for Virtual Environment and Teleoper-*

- ator Systems, 2005. World Haptics 2005. First Joint*, pages 195 – 201, 2005.
- [14] N. Hogan, H.I. Krebs, J. Charnnarong, P. Srikrishna, and A. Sharon. Mit-manus: a workstation for manual therapy and training. i. In *Robot and Human Communication, 1992. Proceedings., IEEE International Workshop on*, pages 161 –165, September 1992.
- [15] Furui Wang, D.E. Barkana, and N. Sarkar. Impact of visual error augmentation when integrated with assist-as-needed training method in robot-assisted rehabilitation. *Neural Systems and Rehabilitation Engineering, IEEE Transactions on*, 18(5):571 –579, 2010.
- [16] Aykut Cihan Satici, Ahmetcan Erdogan, and Volkan Patoglu. A multi-lateral rehabilitation system. *Turkish Journal of Electrical Engineering and Computer Sciences*, 2010.
- [17] Yili Fu, Fuxiang Zhang, Shuguo Wang, and Qinggang Meng. Development of an embedded control platform of a continuous passive motion machine. In *Intelligent Robots and Systems, 2006 IEEE/RSJ International Conference on*, pages 1617 –1622, 2006.
- [18] K. Ikeda. Quantitative evaluation of pain by analyzing non-invasively obtained physiological data with particular reference to joint healing with continuous passive motion. In *Engineering in Medicine and Biology Society, 1995 and 14th Conference of the Biomedical Engineering Society of India. An International Meeting, Proceedings of the First Regional Conference., IEEE*, pages 3/25 –3/26, February 1995.

- [19] B. Vanderborght, N.G. Tsagarakis, C. Semini, R. Van Ham, and D.G. Caldwell. Macepa 2.0: Adjustable compliant actuator with stiffening characteristic for energy efficient hopping. In *Robotics and Automation, 2009. ICRA '09. IEEE International Conference on*, pages 544–549, may 2009.
- [20] R. Ekkelenkamp, J. Veneman, and H. van der Kooij. Lopes: a lower extremity powered exoskeleton. In *Robotics and Automation, 2007 IEEE International Conference on*, pages 3132–3133, 2007.
- [21] Yanfang Li, J.C. Huegel, V. Patoglu, and M.K. O'Malley. Progressive shared control for training in virtual environments. In *EuroHaptics conference, 2009 and Symposium on Haptic Interfaces for Virtual Environment and Teleoperator Systems. World Haptics 2009. Third Joint*, pages 332–337, 2009.
- [22] B. Graf and R.D. Schraft. Behavior-based path modification for shared control of robotic walking aids. In *Rehabilitation Robotics, 2007. ICORR 2007. IEEE 10th International Conference on*, pages 317–322, 2007.
- [23] Robert Riener, Lars Lünenburger, and Gery Colombo. Human-Centered Robotics Applied to Gait Training and Assessment. *Veterans Admin. Journal of Rehabilitation Research and Development*, 2006.
- [24] G. Colombo, M. Joerg, R. Schreier, and V. Dietz. Treadmill training of paraplegic patients using a robotic orthosis. *Journal of Rehabilitation Research and Development*, 37(6):693–700, 2000.
- [25] Jan Frederik Veneman. *Design and evaluation of the gait rehabilitation robot LOPES*. PhD thesis, Enschede, December 2007.

- [26] Constantinos Mavroidis, Jason Nikitzuk, Brian Weinberg, Gil Dana-her, Katherine Jensen, Philip Pelletier, Jennifer Prugnarola, Ryan Stu-  
art, Roberto Arango, Matt Leahey, Robert Pavone, Andrew Provo, and  
Dan Yasevac. Smart portable rehabilitation devices. *Journal of Neuro-  
Engineering and Rehabilitation*, 2(1):18, 2005.
- [27] Jaipur knee. <http://remotiondesigns.org/jaipurknee.html>.
- [28] V. Cai, Ph. Bidaud, V. Hayward, and F. Gosselin. Design of self-  
adjusting orthoses for rehabilitation. In *Proceedings of the 14th IASTED  
International Conference on Robotics and Applications*, pages 215–223,  
2009.
- [29] D.G. Caldwell, C. Favede, and N. Tsagarakis. Dextrous exploration of  
a virtual world for improved prototyping. In *Robotics and Automation,  
1998. Proceedings. 1998 IEEE International Conference on*, volume 1,  
pages 298 –303 vol.1, may 1998.
- [30] C. Carignan, M. Liszka, and S. Roderick. Design of an arm exoskeleton  
with scapula motion for shoulder rehabilitation. In *Advanced Robotics,  
2005. ICAR '05. Proceedings., 12th International Conference on*, pages  
524 –531, 2005.
- [31] Matjaz Mihelj, Tobias Nef, and Robert Riener. A novel paradigm for  
patient-cooperative control of upper-limb rehabilitation robots. *Ad-  
vanced Robotics*, 21(8):843–867, 2007.
- [32] T. Nef, M. Mihelj, G. Kiefer, C. Perndl, R. Muller, and R. Riener.  
Armin - exoskeleton for arm therapy in stroke patients. In *Rehabilitation*

*Robotics, 2007. ICORR 2007. IEEE 10th International Conference on*, pages 68–74, 2007.

- [33] T. Nef, M. Guidali, and R. Riener. Armin iii - arm therapy exoskeleton with an ergonomic shoulder actuation. *Applied Bionics and Biomechanics*, 2(6):127–142, 2009.
- [34] Wenbin Chen, Caihua Xiong, Ronglei Sun, and Xiaolin Huang. On the design of exoskeleton rehabilitation robot with ergonomic shoulder actuation mechanism. In *Proceedings of the 2nd International Conference on Intelligent Robotics and Applications, ICIRA '09*, pages 1097–1110, Berlin, Heidelberg, 2009. Springer-Verlag.
- [35] L. Blankevoort, R. Huiskes, and A. de Lange. The envelope of passive knee joint motion. *Journal of Biomechanics*, 21(9):705 – 709, 711–720, 1988.
- [36] J. Bellmans, J. Bellemans, and M. D. D Ries. *Total Knee Arthroplasty: A Guide to Get Better Performance*, pages 130–134. Springer Berlin Heidelberg, hardbound edition, july 2005.
- [37] C. Carignan, M. Liszka, and S. Roderick. Design of an arm exoskeleton with scapula motion for shoulder rehabilitation. In *Advanced Robotics, 2005. ICAR '05. Proceedings., 12th International Conference on*, pages 524–531, 2005.
- [38] R.J. Sanchez, Jiayin Liu, S. Rao, P. Shah, R. Smith, T. Rahman, S.C. Cramer, J.E. Bobrow, and D.J. Reinkensmeyer. Automating arm movement training following severe stroke: Functional exercises with quantitative feedback in a gravity-reduced environment. *Neural Systems and*

*Rehabilitation Engineering, IEEE Transactions on*, 14(3):378–389, sept. 2006.

- [39] A.H.A. Stienen, E.E.G. Hekman, F.C.T. Van der Helm, G.B. Prange, M.J.A. Jannink, A.M.M. Aalsma, and H. Van der Kooij. Dampace: dynamic force-coordination trainer for the upper extremities. In *Rehabilitation Robotics, 2007. ICORR 2007. IEEE 10th International Conference on*, pages 820–826, 2007.
- [40] A. Frisoli, M. Bergamasco, M.C. Carboncini, and B. Rossi. Robotic assisted rehabilitation in virtual reality with the l-exos. *Stud Health Technol Inform*, 145:40–54, 2009.
- [41] H. Krebs, M. Ferraro, S. Buerger, M. Newbery, A. Makiyama, M. Sandmann, D. Lynch, B. Volpe, and N. Hogan. Rehabilitation robotics: pilot trial of a spatial extension for mit-manus. *Journal of NeuroEngineering and Rehabilitation*, 1(1):5, 2004.
- [42] R.C.V Loureiro and W.S Harwin. Robot aided therapy: Challenges ahead for upper limb stroke rehabilitation. New College, Oxford, UK, September 2004. 5th International Conference on Disability, Virtual Reality and Associated Technologies.
- [43] P. Lammertse, E. Frederiksen, and B. Ruiters. The hapticmaster, a new high-performance haptic interface. In *Proceedings of Eurohaptics 2002*, Edinburgh, UK, 2002.
- [44] S. Hesse, H. Schmidt, C. Werner, C. Rybski, U. Puzich, and A. Bardeleben. A new mechanical arm trainer to intensify the upper limb

- rehabilitation of severely affected patients after stroke: design, concept and first case series. *Eura Medicophys*, 43(4):463–8, December 2007.
- [45] Y.L. Chen, T.S. Kuo, and W.H. Chang. Aid training system for upper extremity rehabilitation. In *Engineering in Medicine and Biology Society, 2001. Proceedings of the 23rd Annual International Conference of the IEEE*, volume 2, pages 1360 – 1363, 2001.
- [46] A. Peattie, Korevaar A., Wilson J., Sandilands B., Chen X.Q., and M. King. Automated variable resistance system for upper limb rehabilitation. *Australasian Conference on Robotics and Automation (ACRA)*, December 2009.
- [47] G.C. Burdea, D. Cioi, J. Martin, D. Fensterheim, and M. Holenski. The rutgers arm ii rehabilitation system—a feasibility study. *Neural Systems and Rehabilitation Engineering, IEEE Transactions on*, 18(5):505–514, 2010.
- [48] N. Mumford, J. Duckworth, R. Eldridge, M. Guglielmetti, P. Thomas, D. Shum, H. Rudolph, G. Williams, and P.H. Wilson. A virtual tabletop workspace for upper-limb rehabilitation in traumatic brain injury (tbi): A multiple case study evaluation. In *Virtual Rehabilitation, 2008*, pages 175–180, 2008.
- [49] J.-P. Merlet. *Parallel Robots*. Springer, 2 edition, 2006.
- [50] Kyung-Lyong Han, Oh Kyu Choi, In Lee, Inwook Hwang, J.S. Lee, and Seungmoon Choi. Design and control of omni-directional mobile robot for mobile haptic interface. In *Control, Automation and Systems, 2008. ICCAS 2008. International Conference on*, pages 1290–1295, 2008.

- [51] G. A. Pratt and M. M. Williamson. Series elastic actuators. In *IEEE International Conference on Intelligent Robots and Systems*, 1995.
- [52] J. E. Pratt, B. T. Krupp, C. J. Morse, and S. H. Collins. The RoboKnee: an exoskeleton for enhancing strength and endurance during walking. In *IEEE International Conference on Robotics & Automation*, 2004.
- [53] J. F. Veneman, R. Ekkelenkamp, R. Kruidhof, F. C. T. van der Helm, and H. van der Kooij. A Series Elastic- and Bowden-Cable-Based Actuation System for Use as Torque Actuator in Exoskeleton-Type Robots. *The International Journal of Robotics Research*, 25(3):261–281, 2006.
- [54] H. Herr and A. Wilkenfeld. User-adaptive Control of a Magnetorheological Prosthetic Knee. *Industrial Robot: An International Journal*, 30(1):42–55, 2003.
- [55] D. Paluska and H. Herr. The Effect of Series Elasticity on Actuator Power and Work Output: Implications for Robotic and Prosthetic Joint Design. *Robotics and Autonomous Systems*, 54:667–673, 2006.
- [56] G. A. Pratt. Low Impedance Walking Robots. *Integrative and Comparative Biology*, 42(1):174–181, 2002.
- [57] D. W. Robinson, J. E. Pratt, D. J. Paluska, and G. A. Pratt. Series elastic actuator development for a biomimetic walking robot. In *IEEE/ASME International Conference on Advance Intelligent Mechatronics*, 1999.
- [58] S. Eppinger and W. Seering. Understanding bandwidth limitations in robot force control. In *Robotics and Automation. Proceedings. 1987*

- IEEE International Conference on*, volume 4, pages 904 – 909, mar 1987.
- [59] Byoung Hun Kang, J.T. Wen, N.G. Dagalakis, and J.J. Gorman. Analysis and design of parallel mechanisms with flexure joints. In *Robotics and Automation, 2004. Proceedings. ICRA '04. 2004 IEEE International Conference on*, volume 4, pages 4097 – 4102 Vol.4, 26-may 1, 2004.
- [60] C.E. English and D. Russell. Mechanics and stiffness limitations of a variable stiffness actuator for use in prosthetic limbs. *Mechanism and Machine Theory*, 34(1):7–25, 1999.
- [61] A. Bicchi and G. Tonietti. Fast and "soft-arm" tactics [robot arm design]. *IEEE Robotics Automation Magazine*, 11(2):22–33, 2004.
- [62] R. Schiavi, G. Grioli, S. Sen, and A. Bicchi. VSA-II: A novel prototype of variable stiffness actuator for safe and performing robots interacting with humans. In *IEEE International Conference on Robotics and Automation*, pages 2171 –2176, May 2008.
- [63] Shane A. Migliore, Edgar A. Brown, and Stephen P. DeWeerth. Novel nonlinear elastic actuators for passively controlling robotic joint compliance. *Journal of Mechanical Design*, 129(4):406–412, 2007.
- [64] J. Yamaguchi, D. Nishino, and A. Takanishi. Realization of dynamic biped walking varying joint stiffness using antagonistic driven joints. In *IEEE International Conference on Robotics and Automation*, volume 3, pages 2022–2029, May 1998.
- [65] F. Petit, M. fChalon, W. Friedl, M. Grebenstein, A.A. Schaffer, and G. Hirzinger. Bidirectional antagonistic variable stiffness actuation:

- Analysis, design and implementation. In *IEEE International Conference on Robotics and Automation*, pages 4189–4196, May 2010.
- [66] Milton A. Chace. *Development and application of vector mathematics for kinematic analysis of three-dimensional mechanisms*. PhD thesis, University of Michigan, 1964.
- [67] P. Viboonchaicheep, A. Shimada, and Y. Kosaka. Position rectification control for mecanum wheeled omni-directional vehicles. In *Industrial Electronics Society, 2003. IECON '03. The 29th Annual Conference of the IEEE*, volume 1, pages 854 – 859 vol.1, 2003.
- [68] Thomas R. Kane and David A. Levinson. The Use of Kane’s Dynamical Equations in Robotics. *The International Journal of Robotics Research*, 2(3):3–21, 1983.
- [69] D. Octomo, Hwee Choo Liaw, G. Alici, and B. Shirinzadeh. Direct kinematics and analytical solution to 3rrr parallel planar mechanisms. In *Control, Automation, Robotics and Vision, 2006. ICARCV '06. 9th International Conference on*, pages 1 –6, dec. 2006.
- [70] J. W. Sensinger and R. F. ff. Weir. Improvements to series elastic actuators. In *IEEE/ASME International Conference on Mechatronic and Embedded Systems and Applications*, 2006.
- [71] G. A. Pratt, P. Williamson, C. Bolton, and A. Hofman. Late Motor Processing in Low-Impedance Robots: Impedance Control of Series Elastic Actuators. In *American Control Conference*, 2004.

- [72] G. Wyeth. Demonstrating the safety and performance of a velocity sourced series elastic actuator. In *IEEE International Conference on Robotics and Automation*, 2008.
- [73] H. Vallery, J. Veneman, E. van Asseldonk, R. Ekkelenkamp, M. Buss, and H. van Der Kooij. Compliant actuation of rehabilitation robots. *IEEE Robotics & Automation Magazine*, 15(3):60–69, 2008.
- [74] P.Y. Li and R. Horowitz. Control of smart exercise machines. i. problem formulation and nonadaptive control. *Mechatronics, IEEE/ASME Transactions on*, 2(4):237–247, December 1997.
- [75] P.Y. Li and R. Horowitz. Passive velocity field control of mechanical manipulators. *Robotics and Automation, IEEE Transactions on*, 15(4):751–763, August 1999.
- [76] P.Y. Li and R. Horowitz. Passive velocity field control (pvfc). part i. geometry and robustness. *Automatic Control, IEEE Transactions on*, 46(9):1346–1359, September 2001.
- [77] Dongjun Lee and P.Y. Li. Passive bilateral control and tool dynamics rendering for nonlinear mechanical teleoperators. *Robotics, IEEE Transactions on*, 21(5):936–951, October 2005.
- [78] Dongjun Lee and P.Y. Li. Passive bilateral feedforward control of linear dynamically similar teleoperated manipulators. *Robotics and Automation, IEEE Transactions on*, 19(3):443–456, June 2003.
- [79] J. Moreno-Valenzuela. On passive velocity field control of robot arms. In *Decision and Control, 2006 45th IEEE Conference on*, pages 2955–2960, December 2006.

- [80] Javier Moreno-Valenzuela. Velocity field control of robot manipulators by using only position measurements. *Journal of the Franklin Institute*, 344(8):1021 – 1038, 2007.
- [81] Ahmetcan Erdogan and Volkan Patoglu. Passive velocity field control of a forearm-wrist rehabilitation robot. In *International Conference on Rehabilitation Robotics (ICORR2011)*, 2011.
- [82] Ahmetcan Erdogan and Volkan Patoglu. Online generation of velocity fields for passive contour following. In *IEEE World Haptics Conference (WHC2011)*, 2011.
- [83] Jean-Jacques Slotine and Weiping Li. *Applied Nonlinear Control*. Prentice Hall, October 1990.
- [84] N. Sadegh and R. Horowitz. Stability and robustness analysis of a class of adaptive controllers for robotic manipulators. *International Journal of Robotics Research*, 9(3):74–92, June 1990.
- [85] R. Ortega and M. Spong. Adaptive motion control of rigid bodies. *Automatica*, Nov 1989.
- [86] P.Y. Li and R. Horowitz. Passive velocity field control (pvfc). part ii. application to contour following. *Automatic Control, IEEE Transactions on*, 46(9):1360 –1371, September 2001.